

# Discovery and Development of S6821 and S7958 as Potent TAS2R8 Antagonists

Joseph R. Fotsing,\* Vincent Darmohusodo, Andrew P. Patron, Brett W. Ching, Thomas Brady, Melissa Arellano, Qing Chen, Timothy J. Davis, Hanghui Liu, Guy Servant, Lan Zhang, Mark Williams, Michael Saganich, Tanya Ditschun, Catherine Tachdjian, and Donald S. Karanewsky



Cite This: <https://dx.doi.org/10.1021/acs.jmedchem.0c00388>



Read Online

ACCESS |



Metrics & More

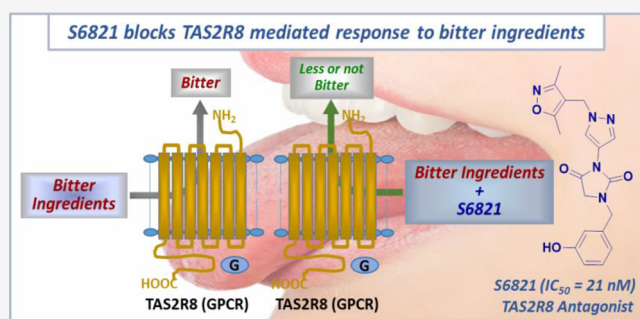


Article Recommendations



Supporting Information

**ABSTRACT:** In humans, bitter taste is mediated by 25 TAS2Rs. Many compounds, including certain active pharmaceutical ingredients, excipients, and nutraceuticals, impart their bitter taste (or in part) through TAS2R8 activation. However, effective TAS2R8 blockers that can either suppress or reduce the bitterness of these compounds have not been described. We are hereby reporting a series of novel 3-(pyrazol-4-yl) imidazolidine-2,4-diones as potent and selective TAS2R8 antagonists. In human sensory tests, S6821 and S7958, two of the most potent analogues from the series, demonstrated efficacy in blocking TAS2R8-mediated bitterness and were selected for development. Following data evaluation by expert panels of a number of national and multinational regulatory bodies, including the US, the EU, and Japan, S6821 and S7958 were approved as safe under conditions of intended use as bitter taste blockers.



## INTRODUCTION

Taste and taste modulation research has long been driven by sensory evaluation with the tongue as the sole testing tool. It was not until recently, with the discovery and characterization of many vertebrate taste receptors,<sup>1–3</sup> that taste research has evolved to using high-throughput screening assays and medicinal chemistry tools to identify and optimize ligands (agonists, antagonists, and positive allosteric modulators) that interact with taste receptors to impart specific taste modalities (Figure 1).<sup>1,2,4–9</sup> Tremendous progress has been made toward the understanding of the taste signaling mechanism<sup>1,2,4,8–12</sup> and the development of assays to evaluate the response of taste receptors to various ligands. Umami and sweet tastes are mediated by TAS1R1/TAS1R3 and TAS1R2/TAS1R3, respectively, which are heterodimeric G-protein coupled receptors (GPCRs).<sup>13</sup> Sour and salty tastes, for their part, are believed to be mediated by ion channels.<sup>8,9,12,14</sup> Early research suggested that the dimeric complex PKD1L3/PKD2L1, a member of the TRP family of ion channels, is a potential candidate receptor for sour taste.<sup>15</sup> However, Horio et al. later demonstrated that PKDs only contribute partly to the detection of sour taste in mice, thus pointing at the involvement of other receptors in sour taste mediation.<sup>16</sup> More recently, the work by Tu et al. identified otopetrin1 (OTOP1), a proton permeable protein that also plays a key role in the formation of gravity-sensing calcium carbonate crystals in the utricle of the ear, as being the sour taste receptor.<sup>8,9,17–19</sup> For

salt taste perception in rodents, ENaC has been shown to participate, at least partially, but it does not seem to play a significant role in human salt taste perception.<sup>14</sup> Other candidate salt receptors are still under evaluation.

Strikingly, bitter taste is mediated by a large family of GPCRs called TAS2Rs (or T2Rs).<sup>20–24</sup> A single TAS2R can recognize a diverse variety of bitter ligands, and a bitter compound can activate multiple TAS2Rs.<sup>5,7,25,26</sup> Bitter taste receptors are present throughout the body and believed to be also implicated in nontaste related roles, including the mediation of many human health conditions and diseases.<sup>27–38</sup> Humans have 25 full-length TAS2Rs, which are highly divergent in sequence, sharing only 30–70% amino acid homology.<sup>39</sup> Additionally, there are more than 150 single nucleotide polymorphisms among individual TAS2R genes,<sup>3,40–43</sup> several of which are responsible for variation in the liking and in the intensity of human bitter taste perception of various bitter tastants.<sup>43–55</sup> For TAS2R8, there are 5 known variants causing amino acid changes.<sup>40,56</sup> Those variants add more diversity to the already complex machinery of bitter taste

Received: March 5, 2020



that fraction F4 mainly and strongly activated TAS2R8 and TAS2R14. Dose–response curves of F4 activation of TAS2R8 and TAS2R14 were subsequently generated (Figure 2). It is

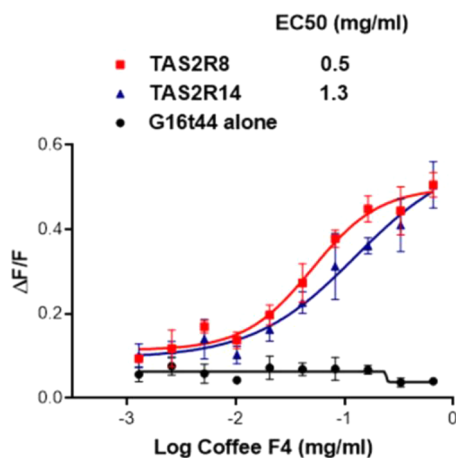


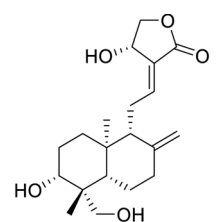
Figure 2. Activation of TAS2R8 and TAS2R14 by coffee fraction F4.

worth noting that TAS2R8 is not one of the bitter taste receptors previously reported to be activated by caffeine, namely, TAS2R7, TAS2R10, TAS2R14, TAS2R43, and TAS2R46.<sup>7</sup> Interestingly, caffeine is believed to contribute to less than 20% of overall coffee bitterness.<sup>78</sup> Hence, based on our data, we hypothesized that TAS2R8 antagonists may significantly reduce the perceived bitterness of coffee.

**Library Screening and Background SAR.** Using a typical microtiter plate FLIPR calcium mobilization assay developed with recombinant cells overexpressing TAS2R8 and a promiscuous G protein,<sup>79</sup> we screened a collection of over 200000 compounds from our corporate collection for antagonist activity on TAS2R8. For the purpose of screening, andrographolide (Figure 3) was used as the surrogate TAS2R8 agonist in the assay; the concentration of andrographolide used in the screening was set to its EC80 value.

Our initial screening campaign identified about 500 compounds (0.25% hit rate) demonstrating at least 50% inhibition of the andrographolide agonist activity at 10  $\mu$ M. Subsequent confirmation and dose–response assays further refined the hit list to 9 compounds with the greatest potency (0.005% of initial library). The most potent compound was S5033 with an IC<sub>50</sub> of 2.3  $\mu$ M in the assay (Figure 4). Following the identification of S5033, we conducted a cluster analysis of the initial 500 primary hits to identify S5033-related analogues. A structure activity relationship (SAR) analysis of the S5033-related analogues revealed that compounds featuring the pyrazolylmethyl-3,5-dimethylisoxazole moiety, depicted as “A”, (Figure 4) exhibit high TAS2R8 antagonist activity relative to the other S5033 analogues. Although not extensively investigated, any change on “A” resulted in a significant decrease in activity. A snapshot of the representative analogues showcasing modifications on moiety “A” and their impacts on the compounds’ activity is provided in the Supporting Information. This article will focus on optimization efforts based on systematic modifications of the linker and “B” moiety.

**Optimization Based on the B moiety.** To quickly evaluate the SAR around modifications of the B moiety, a small library of compounds with generic structure 7 was generated by reacting 1-((3,5-dimethylisoxazol-4-yl)methyl)-1H-pyrazol-



Andrographolide  
TAS2R8 EC50 = 110  $\mu$ M

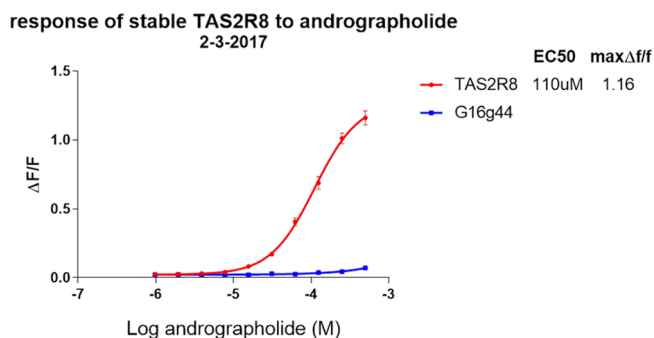


Figure 3. Andrographolide structure and activation of TAS2R8.

4-amine hydrochloride 6 with a set of more than 120 commercially available carboxylic acids. The carboxylic acids were selected so that the corresponding amide coupling products 7 would have a clogP < 4 and a molecular weight <400. The selection also included a variety of appending substituents in order to increase the diversity. It is worth mentioning that the above-mentioned clogP and molecular weight criteria were selected primarily for achieving good solubility. Since the bitter taste receptors are located at the upper surface of the tongue and are thus readily accessible, we prefer compounds with rather poor bioavailability as a means to minimizing unnecessary systemic exposure. The key building block 6 was generated following the sequence of reactions depicted in Scheme 1. In brief, compound 3 was conveniently prepared from commercially available 4-(chloromethyl)-3,5-dimethylisoxazole 1 and ethyl 1H-pyrazole-4-carboxylate 2. Treatment of 3 with hydrazine in ethanol under refluxing conditions yielded compound 4, which was then treated with acidic sodium nitrite to furnish the acyl azide 5. Finally, Curtius’ rearrangement of 5 in *tert*-BuOH led to the corresponding Boc-protected amine, which was subsequently treated with hydrochloric acid to yield the desired amine hydrochloride building block 6. With the amine building block 6 now in hand, the desired amide library was generated by parallel synthesis by coupling amine 6 and the selected set of carboxylic acids (Scheme 1) followed by HPLC purification.

As shown in the representative set of analogues summarized in Table 1, removing the thioethyl group of S5033 yielded the 3-pyridyl analogue 9, which was found to exhibit almost a 2-fold increase in potency. The 2-pyridyl and 4-pyridyl analogues 8 and 10 were two- and 3-fold less active, respectively, when compared to the 3-pyridyl (9). Replacing the thioethyl group of S5033 with a methoxy group produced compound 11 with almost a 2-fold improvement in potency. Moving the methoxy group to the 4 position (13) and 5 position (12) further improved the potency. It is worth noting that the potency of the 2-methoxy-3-pyridyl analogue 11 was very close to that of

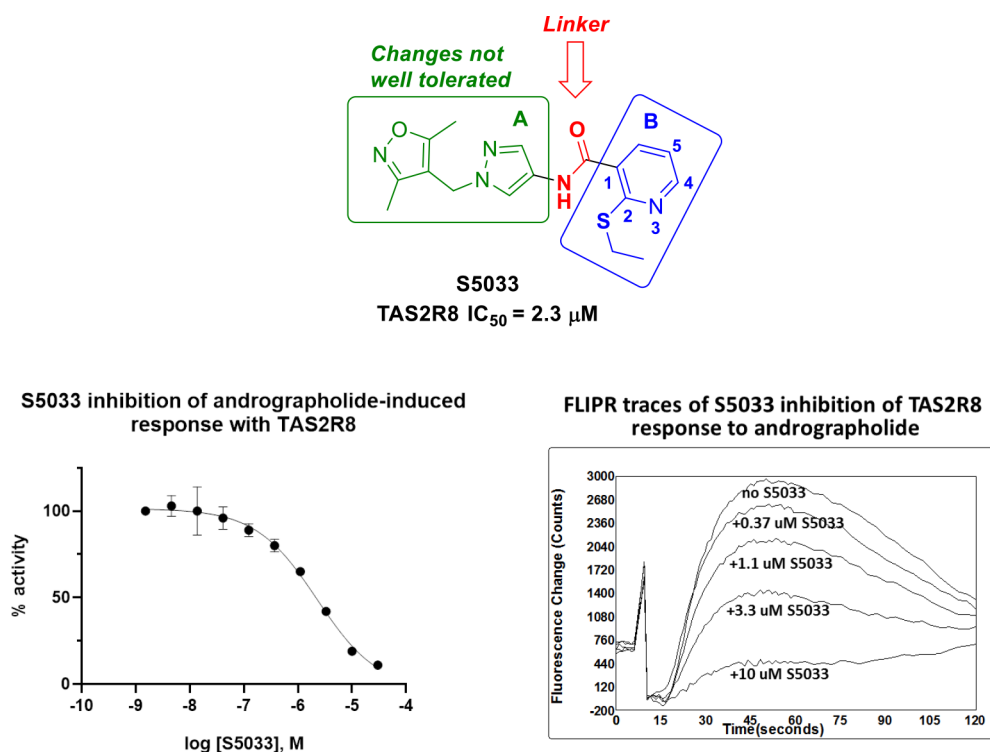
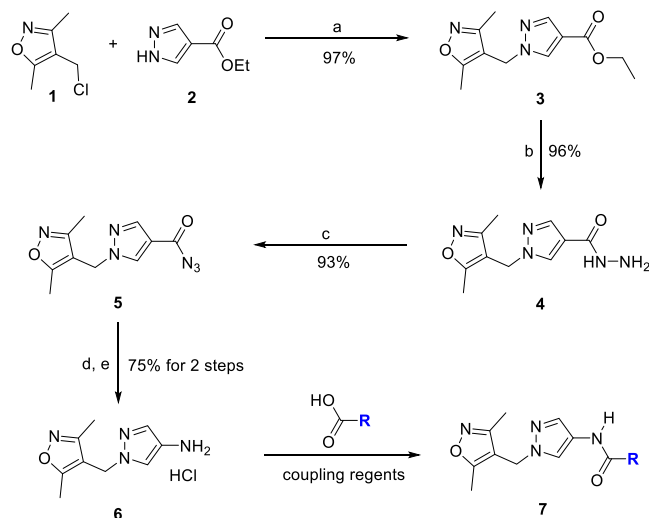


Figure 4. Structure, graphical SAR strategy, and S5033 inhibition of TAS2R8 response to andrographolide.

### Scheme 1. Synthesis of **7** and Generation of Corresponding Library of Amides<sup>a</sup>



<sup>a</sup>Reagents and conditions: (a) Cs<sub>2</sub>CO<sub>3</sub>, DMF, 80 °C, 16 h; (b) N<sub>2</sub>H<sub>4</sub>, EtOH, reflux, 48 h; (c) NaNO<sub>2</sub>, AcOH, H<sub>2</sub>O, 0 °C to room temperature (RT), 30 min; (d) *tert*-BuOH, reflux, 6 h; (e) MeOH, HCl, reflux, 2 h.

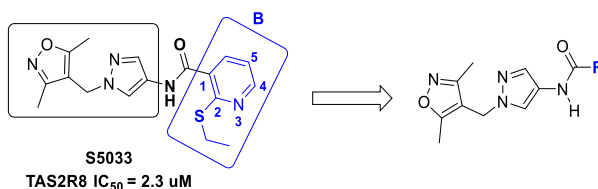
the simple 3-pyridyl analogue **9**. A similar pattern is observed for the simple phenyl series where the activity of **14** remains nearly unchanged with the addition of a methoxy group at the *ortho* position (**15**) but increases to almost 3-fold when the methoxy group is moved to either the *meta* position (**16**) or the *para* position (**17**). Uncapping the methoxy groups to form the corresponding *ortho*-phenol **18**, *meta*-phenol **19**, and *para*-phenol analogues **20**, resulted in a slight increase in potency for all three analogues. We also observed that fused biaryl

analogues such as indole **21**, benzodioxole **23**, and benzodioxine **24** exhibited submicromolar activities. In contrast, the TAS2R8 antagonist activity of the benzoxazole analogue **22** was significantly lower than the other biaryl analogues. Phenyl analogues combining various substituents were also synthesized. While some combinations, such as **25** which combines the **16** and **17** substituents, were not advantageous, others, including **26** (combining **15** and **16** substituents), resulted in compounds with improved potency. Several 5-membered aryl analogues were also synthesized but most of them were only moderately active (e.g., **27**).

While this evaluation provided compounds with good potency in the assay (e.g., **23**), we felt that such level of potency was still insufficient to allow use levels that are low enough to warrant regulatory approval in many parts of the globe as a bitter taste modifying ingredient. Thus, further improvement of potency was deemed necessary. With the valuable SAR insights obtained from these compounds, we moved to the evaluation of the amide linker as a way of finding other opportunities to improve the potency.

**Linker Optimization.** Initial linker modifications were built around compound **14**, which is the core structure of the most potent set of compounds from early evaluations (e.g., **14**–**26**) and would allow us to use a range of commercially available building blocks without the need for laborious syntheses. The set of compounds generated as part of this evaluation is shown in Table 2. Compounds **32**, **33**, and **34** were prepared in the similar manner as in Scheme 1 from the amine **6** and the corresponding carboxylic acids. Compounds **28**–**31**, and **35** were all synthesized in one step by treating the amine hydrochloride building block **6** with the appropriate electrophile in the presence of a base either at room temperature or with heating (Schemes 2a and 2b). In some cases, heating was performed under microwave ( $\mu$ W). Compound **38** was prepared by a base- and heat-promoted

Table 1. Selected SAR Focusing on Substructure B Modifications



Cmpd	R	CLogP	TAS2R8 IC <sub>50</sub> (μM)	Cmpd	R	CLogP	TAS2R8 IC <sub>50</sub> (μM)
8		0.9	2.3	18		2.2	1
9		0.5	1.1	19		1.2	<b>0.4</b>
10		0.5	4.6	20		1.2	<b>0.5</b>
11		1.2	1.1	21		1.7	<b>0.3</b>
12		<b>0.9</b>	<b>0.8</b>	22		1.1	3
13		1.3	0.7	23		1.6	<b>0.2</b>
14		1.5	1.7	24		1.5	<b>0.4</b>
15		1.6	1.9	25		1.3	1
16		1.6	<b>0.7</b>	26		1.6	<b>0.3</b>
17		1.6	<b>0.7</b>	27		0.1	18

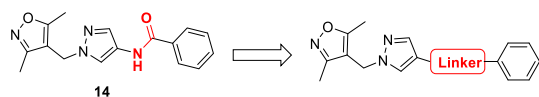
reaction between the benzylurea **35** and ethyl 2-chloro-2-oxoacetate **42** (Scheme 2a). Heating the urea **43** in the presence of a sodium hydride led to the corresponding imidazolidone intermediate **44** that was then reacted with benzyl chloride **45** to furnish **36** (Scheme 2a). Finally, compound **37** was synthesized in two steps starting with the one-pot cascade formation of unsubstituted hydantoin intermediate **48** from acyl azide **5** and the glycine ester **47**, followed by alkylation with benzyl bromide **49** (Scheme 2c).

Screening data collected from these linker modified compounds are summarized in Table 2. Replacing the carboxamide bond of **14** with the sulfonamide to form compound **28** resulted in a loss of activity. Inserting a methylene group between the amide nitrogen and the phenyl ring of **14** to form the isoindolidone **29** induced an even higher drop in potency. However, inserting a carboxyl rather than a methylene group to form the isoindolidone **30** resulted in a significant boost in potency, which was about 8-fold relative to amide **14**. Compounds with improved potencies were also obtained when the phenyl analogue **14** was elongated by insertion of methylene, ethylene, or propylene linkers between the amide carbonyl and the phenyl group, resulting in

compounds **32**, **33**, and **34**, respectively. Within this series of compounds, the two carbon analogue **33** was found to provide greater activity. Thus, we decided to evaluate further modification of the linker without significant alteration of the length with regard to compound **33**. With that in mind, the urea **35** and the corresponding imidazolidinones **36**, **37**, and **38** were synthesized. Although the urea **35**, the imidazolidinone **36**, and the imidazolidinetrione **38** were all less active than **33**, we were pleased to find that the hydantoin **37** exhibited a 2-fold potency improvement relative to **33**. Thus, from this set of analogues targeting optimization of the linker, the isoindolidinone **30** and the hydantoin **37** emerged as the two most potent analogues. Both compounds also have low molecular weights, as desired at this stage of optimization: MW = 322 for **30** and MW = 365 for **37**.

In order to differentiate the two most potent compounds and select the most promising lead for further optimization, solubility and stability data for **30** and **37** were collected (Table 3). The decision to collect high-temperature stability data for these compounds, rather than simple shelf-life stability data, was based on the need for the product candidates to be stable for applications in foods, beverages, and pharmaceuticals

Table 2. Selected SAR Focusing on Linker Modifications



Cmpd	Structure	TAS2R8	CLogP
		IC <sub>50</sub> (μM)	
14		2	1.5
28		4	1.4
29		9	1.7
30		<b>0.2</b>	1.3
31		2	2.0
32		0.8	1.6
33		<b>0.4</b>	2.2
34		0.8	2.5
35		1	1.8
36		1	1.8
37		<b>0.2</b>	0.5
38		2	0.8

that often require harsh processing conditions. The results were clearly in favor of 37, which showed significantly better stability, with 60% of the parent compound remaining after 24 h at 100 °C, pH 7.1 and >99% remaining after 24 h at 100 °C, pH 2.8. Under the same conditions, 30 was significantly less stable, where 5% was remaining after 24 h at 100 °C and pH 7.1 and 3% remaining after 24 h at 100 °C and pH 2.8. In addition, with 12 μM solubility in a pH 7.1 buffer, the isoindolidione 30 was about five times less soluble than the hydantoin 37, which exhibited a 70 μM solubility under the same conditions (Table 3). In light of these results, the hydantoin 37 was selected as the lead compound for further optimization.

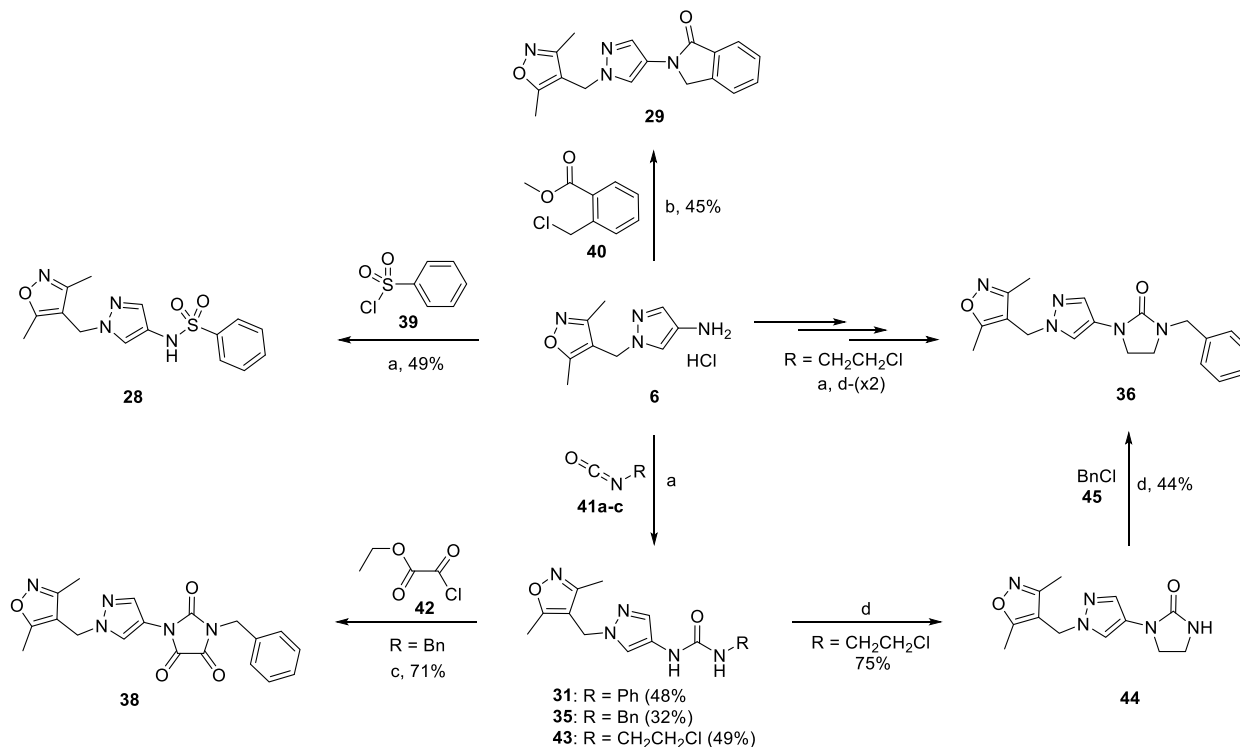
**SAR Refinement of the Lead Compound 37.** With 37 now identified as the lead compound for further SAR refinement, we decided to focus further modifications first on the decoration of the benzyl group of 37 with small substituents (e.g., 51–60) and the replacement of the benzene ring with a variety of five- and six-membered alkyl and aryl rings (e.g., 61–65). Thus, a small diverse library of about 50

analogues was generated. Selected members of the library are shown in Table 4. For the synthesis of the desired analogues, the key building block 48 was scaled up following the procedure depicted in Schemes 2a–2c and then alkylated under basic conditions using the appropriate building blocks (Scheme 3). In cases where the substituent R was an ester, the products were hydrolyzed to furnish the corresponding phenols (e.g., 55 and 56) or carboxylic acids (e.g., 58). Alternatively, 55 and 56 were prepared as in Scheme 5 with or without protection of the phenol; however, using a protecting group clearly improved both the yield and impurity profiles. The latter carboxylic acid 58 was further modified by amide coupling to yield analogues such as 59.

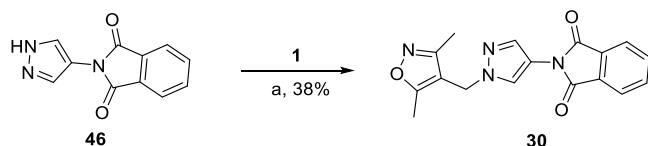
As far as TAS2R8 antagonist activity is concerned, a benzyl group with small substituents such as fluorine, methyl, methoxy, cyano, and hydroxyl was, in general, well tolerated (51–56, Table 4); however, some (e.g., 54) were less active than the lead compound 37. However, the hydroxyl group appeared to be a substituent of choice, exhibiting double digit nanomolar IC<sub>50</sub> values regardless of its position on the benzyl ring: 55, 56, and S6821 (Table 4 and Figure 5). The introduction of carboxylic acid substituents (e.g., 58) resulted in a drop of activity, whereas the corresponding esters (e.g., 57) and small amides such as 59 improved the activity slightly when compared to the lead compound 37; however, it is still less potent than the corresponding hydroxyl analogues. Extending the hydroxyl group to form hydroxyl-methyl analogues (e.g., 60) resulted in a moderate drop of activity. Alternatively, the phenyl ring of the benzyl group was also replaced either with cycloalkyls (e.g., 62), heterocycloalkyls (e.g., 63), or heteroaryls (e.g., 61, 64, and 65). While the cyclohexylmethyl 62 retained the potency, the tetrahydrofurylmethyl 63 was about 5-fold less potent than the lead compound 37. On the other hand, the pyridylmethyl 61, the pyrrolylmethyl 64, and the oxazolylmethyl 65 were all reasonably well tolerated.

With this set of highly potent analogues identified, it was necessary to assess them against the desired characteristics of potential product candidates. For optimal use level and safety margin, the compounds of interest were required to display high *in vitro* TAS2R8 antagonist activity with at least a two-digit nanomolar IC<sub>50</sub> obtained from averaging several sets of data from different screening days. To allow for a convenient formulation in various media, the solubility at pH 7.1 was required to be at least 50 μM and 1000 times greater than the IC<sub>50</sub>. The desired compounds were also required to exhibit less than 5% degradation under most standard processing conditions, which include retorting (up to 60 min at 124 °C) and ultra-high-temperature processing (UHT, 30 s at 140 °C). Ultimately, the compound should exhibit an excellent safety profile. With this set of characteristics in mind, a sequential profiling of our most potent compounds, including compounds 51, 53, and S6821 (Table 4), was undertaken.

Like 51 and 53, some compounds exhibiting the desired potency had solubility far less than the desired 1000 times IC<sub>50</sub> (Table 4). Thus, these compounds were not further considered. Since compound S6821 satisfied both potency and solubility requirements, its stability was assessed under a variety of storage and processing conditions. The results are summarized in Table 5. In fact, while S6821 was very stable under most of the conditions tested, considerable degradation was observed when a solution of S6821 at pH 7.1 was heated either at 100 °C for 24 h or for 60 min at 124 °C. Degradation

Scheme 2a. Synthesis of Compounds 28, 29, 31, 35, 36, and 38<sup>a</sup>

<sup>a</sup>Reagents and conditions: (a) Et<sub>3</sub>N, ACN,  $\mu$ W, 135 °C, 5 min; (b) NaH, DMF,  $\mu$ W, 150 °C, 10 min; (c) Et<sub>3</sub>N, ACN, reflux, 3 h; (d) NaH, ACN,  $\mu$ W, 120 °C, 10 min.

Scheme 2b. Synthesis of Compound 30<sup>a</sup>

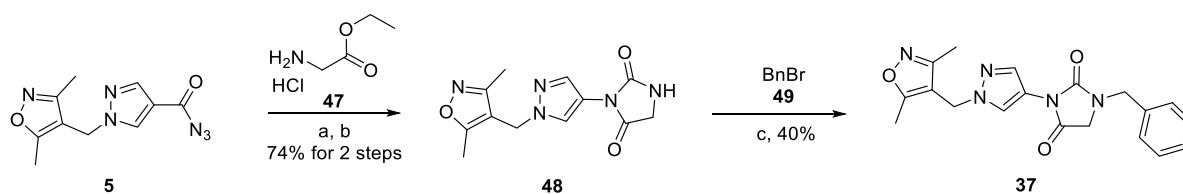
<sup>a</sup>Reagents and conditions: (a) Cs<sub>2</sub>CO<sub>3</sub>, DMF, reflux, 80 °C, 3 h.

of **S6821** was also observed in strongly basic solutions, e.g., ~20% remaining in pH 9.3 after 24 h at RT. In all these cases, the degradative pathway was found to be the hydrolytic opening of the hydantoin ring of **S6821** to form **66**. The latter reaction is, however, reversible, with **66** rapidly cyclizing back to **S6821** below neutral pH (Scheme 4).

To see if the antagonist activity of **S6821** on TAS2R8 was reversible, we conducted a ratiometric calcium imaging experiment using a multichannel perfusion system, so the compounds could be applied reversibly or “washed out” (Figure 6). In a preliminary set of experiments, we first determined that a 5 min washout time by Hank’s balanced salt

solution (HBSS) was sufficient for cells to recover from agonist stimulation with andrographolide (data not shown). Cells were then repeatedly stimulated with either 100  $\mu$ M andrographolide or with 100  $\mu$ M andrographolide and 1  $\mu$ M **S6821** (Figure 6A and B). As expected, 1  $\mu$ M **S6821** significantly blocked the response of all andrographolide responding cells. Furthermore, a complete recovery of the agonist activity was observed following a brief 5 min washout, thus indicating that the binding of **S6821** to TAS2R8 is completely reversible. The same results were also observed using 100  $\mu$ M chloramphenicol and 1  $\mu$ M **S6821** (Figure 7).

Further mechanistic investigations of the **S6821** interaction with TAS2R8 were also conducted. We performed a dose–response analysis of TAS2R8 with increasing concentrations of the agonist chloramphenicol and fixed concentrations of **S6821**. Dose–response curves of TAS2R8 with chloramphenicol alone resulted in an EC<sub>50</sub> of 41  $\mu$ M. Increasing the concentrations of **S6821**, successively, resulted in successive rightward shifts in the chloramphenicol dose–response curves. At **S6821** concentrations above 30 nM, the highest chloramphenicol concentration (2 mM) could not be

Scheme 2c. Synthesis of Compound 37<sup>a</sup>

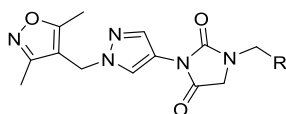
<sup>a</sup>Reagents and conditions: (a) toluene, reflux, 1 h; (b) Et<sub>3</sub>N, toluene, reflux, 16 h; (c) Cs<sub>2</sub>CO<sub>3</sub>, DMF,  $\mu$ W, 85 °C, 20 min.

Table 3. Solubility and Stability of Compounds 30 and 37

Cmpd	Structure	TAS2R8 IC <sub>50</sub> (μM)	CLogP	Solubility (μM)*	% Remaining**	
					pH 7.1	pH 2.8
30		<b>0.2</b>	1.3	12	~5%	~3%
37		<b>0.2</b>	0.5	<b>70</b>	~60%	>99%

\*After 24 h at pH 7.1. \*\*After 24 h at 100 °C.

Table 4. Selected Compounds for Lead Refinement Based on Right Hand Side Modifications



Cmpd	R	TAS2R8 IC <sub>50</sub> (μM)	CLogP	Solubility (μM)*	Sol./IC <sub>50</sub>
50	H	0.9	-1.5		
37		0.2	0.5		
51		<b>0.1</b>	0.7	51	600
52		0.1	1.0		
53		<b>0.1</b>	0.4	16	267
54		0.5	0.1		
55		0.1	-0.2		
<b>S6821</b>		<b>0.02</b>	-0.1	<b>244</b>	<b>11619</b>
56		0.04	-0.1		
57		0.1	0.5		
58		2	0.3		
59		0.1	-0.8		
60		0.3	-0.5		
61		1	-1.0		
62		0.3	1.4		
63		1	-0.7		
64		0.2	-1.1		
65		0.4	-1.1		

\*After 24 h at pH 7.1.

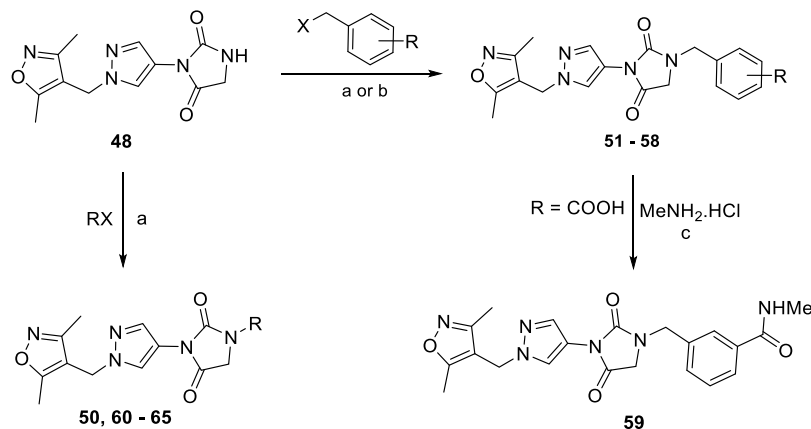
produced; a signal equivalent to the maximum receptor response and higher concentrations of chloramphenicol interfered with the assay. In fact, we observed that at

concentrations above 1–2 mM the assay response begins to decrease. At these high concentrations, either (1) chloramphenicol begins to inhibit TAS2R8 or (2) some other nonspecific inhibitory effect reduces the fluorescent signal. While this observation could suggest an insurmountable noncompetitive mechanism, the dose–response curve fits the convergence to a similar value of E<sub>max</sub>, the equidistant dextral right shifts in the chloramphenicol dose–responses, and the Schild regression analysis point to a surmountable competitive mechanism of action (Figure 8).

**S6821** antagonist profile was also evaluated with transiently transfected cells for relative selectivity against a panel of 16 TAS2Rs, and the results are shown in Figure 9; the list of agonists used for the panel screening and the corresponding TAS2R targets are provided in Table 6. It was determined from these studies that at concentrations up to 25 μM, **S6821** exhibits high TAS2R8 selectivity across the entire panel of the 16 TAS2Rs screened (Figure 9 and Table 6). TAS2R8 activity was inhibited by about 90% in the presence of 25 μM **S6821**, and only TAS2R39 was also poorly antagonized. However, although the effect of 25 μM **S6821** on other TAS2Rs was found to be poor, it would not be surprising to observe a more promiscuous behavior at higher concentrations. In fact, despite the low sequence similarity between TAS2Rs, bitter antagonists reported thus far have been shown to be promiscuous toward a range of TAS2Rs.<sup>67,69</sup>

While the relatively high TAS2R8 selectivity of **S6821** could be viewed as a limitation to its antagonist effect on a broader range of bitter tastants, we hypothesized that this high selectivity could also be a good indication of a limited safety liability for **S6821**. The potential toxicity of **S6821** was initially assessed on the basis of structural alerts and on the basis of safety information available for its component fragments.<sup>80–82</sup> Since the latter assessment did not reveal any structural alerts, **S6821** was not expected to be carcinogenic or mutagenic. In light of these results and given its high potency, selectivity, and solubility as well as its good stability profiles across a number of storage and processing conditions, **S6821** was selected for developmental profiling. **S6821** was not found to be mutagenic or clastogenic *in vitro* and did not induce micronuclei in bone marrow polychromatic erythrocytes *in vivo*.<sup>75</sup> Phase I metabolites **M397A**, **M397B**, and **M397C** resulting from monohydroxylation at various positions of the phenol ring were identified during an *in vitro* metabolism study of **S6821** using rat and human liver microsomes (Scheme 5 and ref 75).

In rat pharmacokinetic (PK) studies, the majority of **S6821** was found to rapidly convert to the corresponding sulfate **M461** and glucuronide **M557** (Scheme 6). Of the phase I

Scheme 3. Synthesis of Selected Compounds 50–65<sup>a</sup>

<sup>a</sup>Reagents and conditions: (a) base, solvent,  $\mu$ W, or conventional heating; (b) condition (a), NaOH, HCl; (c) DIEA, HOBT, EDCI.

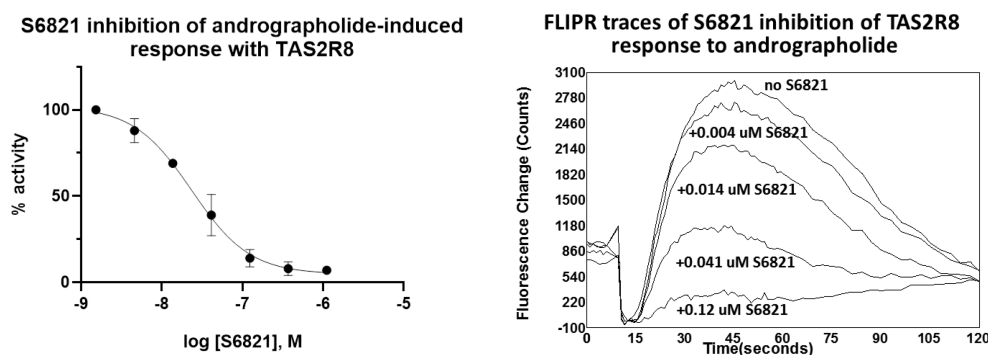


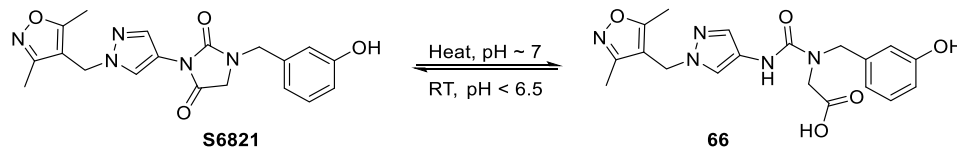
Figure 5. S6821 potently inhibits TAS2R response to andrographolide.

Table 5. Selected Data for S6821

compound	TAS2R8 IC <sub>50</sub> ( $\mu$ M)	solubility ( $\mu$ M) <sup>a</sup>	solubility/IC <sub>50</sub>	stability test conditions			% remaining
				temperature	pH	time	
S6821	0.02	244	11619	RT	2.8	24 h	>99%
				RT	5.0	24 h	>99%
				RT	7.1	24 h	>99%
				RT	9.3	24 h	~20%
				100 °C	2.8	24 h	>99%
				100 °C	5.0	24 h	>99%
				100 °C	7.1	24 h	~55%
				124 °C	6.0	60 min	>99%
				124 °C	7.1	60 min	~89%
				140 °C	6.5	30 s	>99%

<sup>a</sup>After 24 h at pH 7.1.

## Scheme 4. Temperature and pH-Dependent Stability of S6821



metabolites detected *in vitro*, only M397C was detected *in vivo*.<sup>75</sup>

*In vivo* 28-day dose-range-finding toxicity studies of S6821 determined the maximum tolerated dose (MTD) to be above 100 mg/kg/day (the highest dose tested) for CD rats, and no S6821 treatment-related adverse events were observed for the

90-day repeat-dose toxicity study.<sup>75</sup> Thus, the no-observed adverse-effect level (NOAEL) for S6821 was 100 mg/kg of body weight (bw)/day, which was the highest dose tested. S6821 also demonstrated a NOAEL of 1000 mg/kg of bw/day (the highest dose tested) for both maternal toxicity and embryo/fetal development following oral administration to

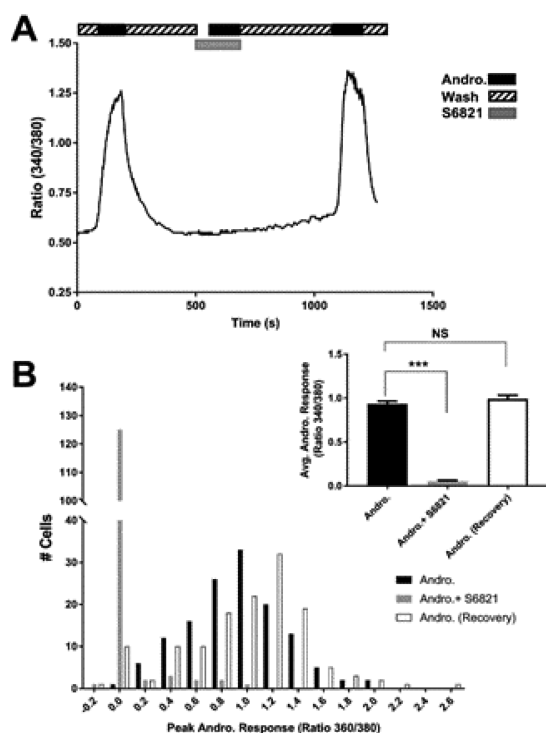


**Figure 6.** S6821 reversibly blocks andrographolide activation of TAS2R8-expressing cells. (A) Representative experiment showing average calcium response of all andrographolide responding cells during repeated 100  $\mu\text{M}$  andrographolide stimulations either with or without inhibitor S6821 (1  $\mu\text{M}$ ). (B) Distribution of peak amplitude of all cells during 3 consecutive andrographolide applications with initial andrographolide application (control, black bars), in the presence of S6821 (gray bars) and following wash-out (recovery, white bars). Average peak ( $\pm$  SEM) responses for the three applications are showed in the inset. Note the significant block of andrographolide by S6821 ( $P < 0.0001$ ,  $n = 136$  cells, two sample  $t$  test). No significant difference was found between the first and the third andrographolide responses ( $P = 0.24$ , two sample  $t$  test), suggesting complete recovery/washout of S6821. Data are from 136 total cells from 3 separate imaging experiments.

pregnant rats during gestation.<sup>75</sup> The detailed ADME-PK, genotoxicity, and toxicity studies conducted as part of the S6821 development campaign have been previously reported.<sup>75</sup> Details of the syntheses of M397A, M397B, and M397C (Scheme 5) as well as M461 and M557 are described herein for the first time.

Since some TAS2R antagonists have been reported to also be agonists of other TAS2Rs,<sup>5</sup> we decided to check if S6821 could be activating other TAS2R(s) in our cell-based assays. Thus, the S6821 TAS2Rs agonist profile was evaluated on transiently transfected cells. The results showed stimulation of TAS2R1 and TAS2R14 at 25  $\mu\text{M}$  S6821. Subsequent dose-response assays on stable cell lines revealed EC<sub>50</sub> values of 150  $\mu\text{M}$  and 40  $\mu\text{M}$  against TAS2R1 and TAS2R14, respectively (Figure 10). S6821 was ultimately sensory-evaluated for intrinsic bitterness and was not significantly bitter up to 150  $\mu\text{M}$ . On a 15-point bitterness scale, 150  $\mu\text{M}$  S6821 scored  $2.8 \pm 0.6$  on average, and panelists found no significant difference in bitterness among low sodium buffer solution (LSB), LSB + 100  $\mu\text{M}$  S6821, and LSB + 150  $\mu\text{M}$  S6821 samples ( $p$ -value  $> 0.05$ ), as shown in Table 7. Hence, at low concentrations, S6821 was expected to effectively block TAS2R8-mediated bitterness without significantly adding

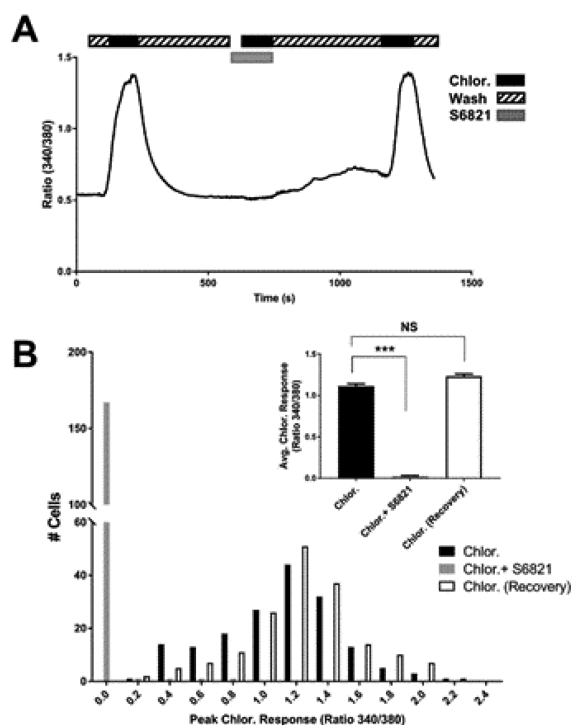


**Figure 7.** S6821 reversibly blocks chloramphenicol activation of TAS2R8-expressing cells. (A) Representative experiment showing average calcium response of all chloramphenicol responding cells during repeated 100  $\mu\text{M}$  chloramphenicol stimulations either with or without inhibitor S6821 (1  $\mu\text{M}$ ). (B) Distribution of peak amplitude of all cells during 3 consecutive chloramphenicol applications with initial chloramphenicol application (control, black bars), in the presence of S6821 (Gray Bars) and following wash-out (Recovery, White Bars). Average peak ( $\pm$  SEM) responses for the three applications are showed in the inset. Note the significant block of chloramphenicol by S6821 ( $P < 0.0001$ ,  $n = 171$  cells, two sample  $t$  test). No reduction was found between the first and the third chloramphenicol responses, suggesting complete recovery/washout of S6821. Data are from 171 total cells from 3 separate imaging experiments.

bitterness through the activation of other TAS2Rs (e.g., TAS2R14).

To assess its bitterness blocking efficacy, S6821 was evaluated in taste tests for the reduction of bitterness in Alta Rica instant coffee. A sample containing 22.5 g of Alta Rica 100% Arabica instant coffee in 750 mL of water and 250 mL of whole milk was first tasted alone and deemed strongly to very strongly bitter by 13 out of 17 panelists. At the same time 3 out of 17 panelists rated the sample as moderately bitter and only 1 out of the 17 panelists found it to be weakly bitter. When the coffee sample was compared to a coffee sample containing 5  $\mu\text{M}$  S6821, more than 78% of responses had the sample containing S6821 as being less bitter, with a  $p$ -value  $< 0.001$  (Figure 11). These results are likely influenced by variations in TAS2Rs genetic coding sequences between panelists. In fact, interindividual genetic polymorphisms have been found to have a significant effect on human sensitivity to and/or liking of coffee.<sup>30,52,54,55</sup>

**SAR Targeting Potent and Soluble Analogues with Broader Stability Profile.** Encouraged by the very positive safety data obtained with S6821, we decided to undertake additional efforts aimed at identifying an analogue with an improved hydrolytic stability profile as a backup for S6821.

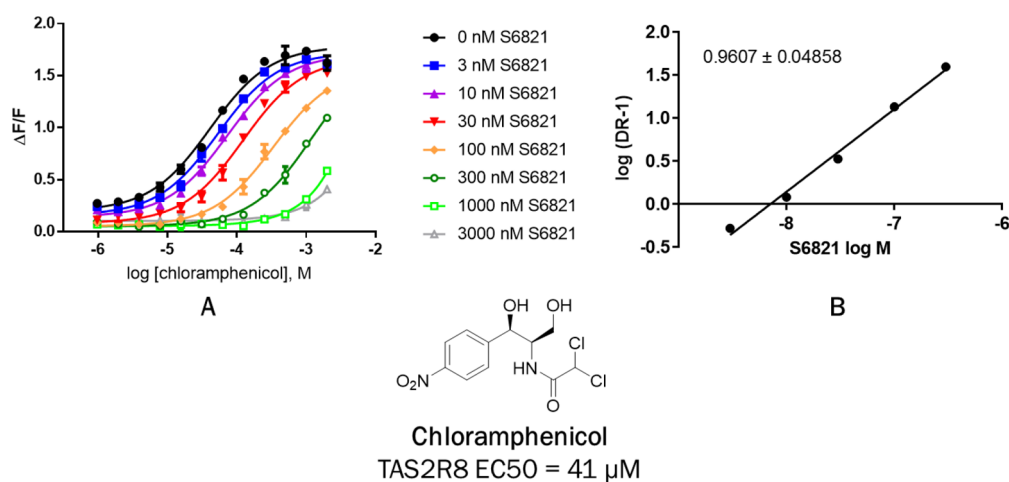


**Figure 8.** S6821 inhibits chloramphenicol activation of TAS2R8 in a competitive manner. (A) TAS2R8-expressing cells were treated with increasing concentrations of chloramphenicol in the absence or presence of 3 nM to 3000 nM S6821, and receptor response was measured in the cell-based assay. Data were calculated as the mean  $\pm$  s.d. of assay duplicates. Similar results were obtained in 3 independent experiments. (B) Schild regression analysis from dose–response curves in panel (A).

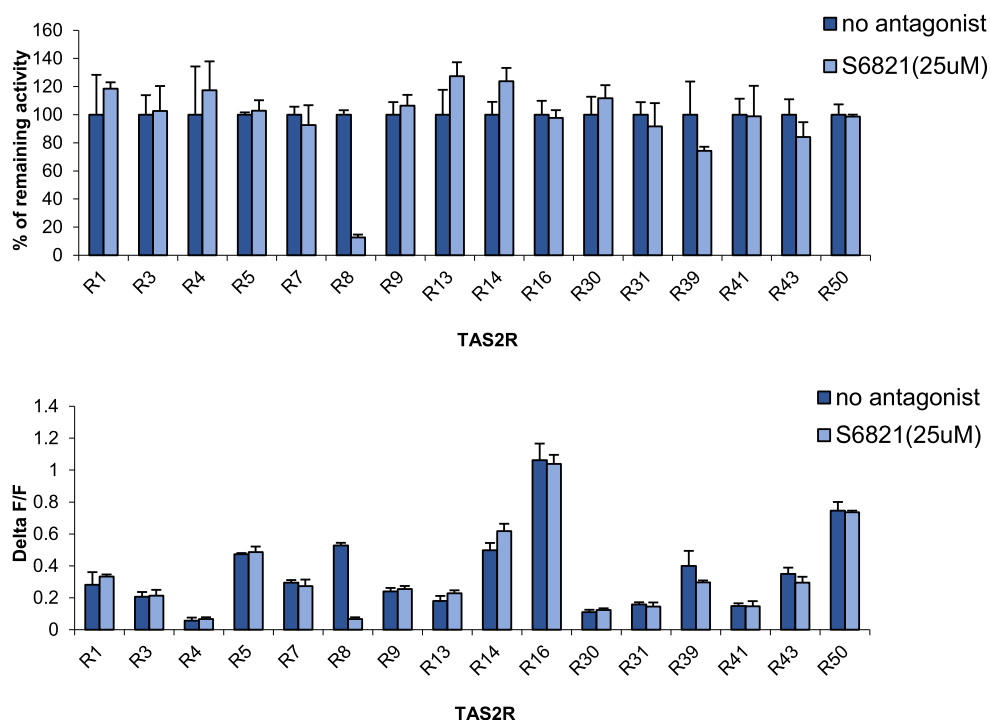


**Figure 9.** TAS2Rs panel screening of S6821 indicates a relatively high selectivity for TAS2R8; refer to Table 6 for details on agonists used.

The strategy was to add substituents to the methylene moiety of the hydantoin ring in order to hinder the access of water and other nucleophiles to the vulnerable carbonyl site and thus slow the hydrolysis of the hydantoin ring. With that in mind, compounds 71–76 were synthesized following the reaction sequence shown in Scheme 5.

Compounds generated were once again screened on stable cells expressing TAS2R8 in the presence of andrographolide as agonist. To our delight, most of the generated compounds retained double digit nanomolar inhibitory activity (Figure 12 and Table 8). In addition, compounds 71–74 and S7958 still met our predefined solubility criteria of at least 50 μM and 1000 times IC<sub>50</sub>. However, the stability of compounds 73 and 74 was unexpectedly low. Arguably, in an aqueous solution, the

hydroxymethyl group present in the latter compounds may coordinate with a water molecule to help drive the hydrolysis of the adjacent carbonyl moiety. Gratifyingly, S7958 suffered less than 1% hydrolysis when heated with pH 7.1 for 24 h at 100 °C and for 60 min at 124 °C (Table 8), which was a significant improvement over S6821 under the same conditions (Table 5 and 8). The impressive hydrolytic stability of S7958 was also evidenced in a strong basic pH, with S7958 exhibiting no noticeable degradation even after 24 h with pH 9.3 at RT. S7958 was also evaluated for antagonist activity on other TAS2Rs and was found to exhibit an inhibition profile that was very similar to that of S6821 (Table 8).

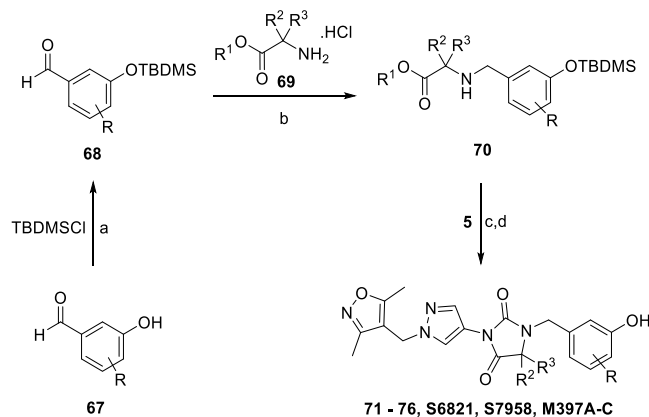
Thus, given the excellent stability, solubility, and TAS2R8 antagonist activity of S7958 and the expectation that it may

Table 6. Panel of TAS2Rs and Corresponding Agonists Used to Access the Putative S6821 and S7958 Antagonist Effect<sup>a</sup>

Receptor	Agonist	Agonist [uM]	25 uM S6821 (% Act remaining)	25 uM S7958 (% Act remaining)
TAS2R1	Picric acid	50	●	●
TAS2R3	Chloroquine	50	●	●
TAS2R4	Chloroquine	5000	●	●
TAS2R5	Picoline	10000	●	●
TAS2R7	Chloroquine	10000	●	●
TAS2R8	Andrographolide	500	●	●
TAS2R9	Ofloxacin	1000	●	●
TAS2R13	Oxyphenonium	1000	●	●
TAS2R14	Aristolochic acid	4	●	●
TAS2R16	Salicin	1000	●	●
TAS2R30	Denatonium	1	●	●
TAS2R31	Aristolochic acid	1	●	●
TAS2R39	Ranitidine	5000	●	●
TAS2R41	Picric acid	10	●	●
TAS2R43	Aristolochic acid	0.05	●	●
TAS2R50	Andrographolide	10	●	●

<sup>a</sup>Relative activity remaining: <25% (green), 25–75% (yellow), >75% (red)

### Scheme 5. Synthesis of 71–76, S6821, S7958, M397A, M397B, and M397C<sup>a</sup>



<sup>a</sup>Reagents and conditions: (a) imidazole or DIEA, DCM; (b) NaBH(OAc)<sub>3</sub>, Et<sub>3</sub>N, DCE; (c) toluene, reflux; (d) aq. HCl.

also exhibit a safety profile similar to that of S6821, we decided to move S7958 into development as a S6821 backup. Subsequent *in vitro* and *in vivo* safety evaluations conducted as part of S7958 development have also been reported.<sup>75</sup> As expected, the ADME-PK, genotoxicity, and toxicity profile of S7958 were all in line with the positive data obtained for S6821, as summarized above. In line with its potency, S7958 also showed a significant block of coffee bitterness in taste test (Table 9).

**Regulatory Status and Evolving Product Application of S6821 and S7958.** In light of these safety and efficacy data, S6821 and S7958 were determined to be “Generally Recognized As Safe” by the Flavor and Extract Manufacturers Association (FEMA) expert panel and were assigned FEMA GRAS Numbers 4725 and 4726,<sup>83,84</sup> respectively. S6821 and S7958 have also been determined to be safe at the current

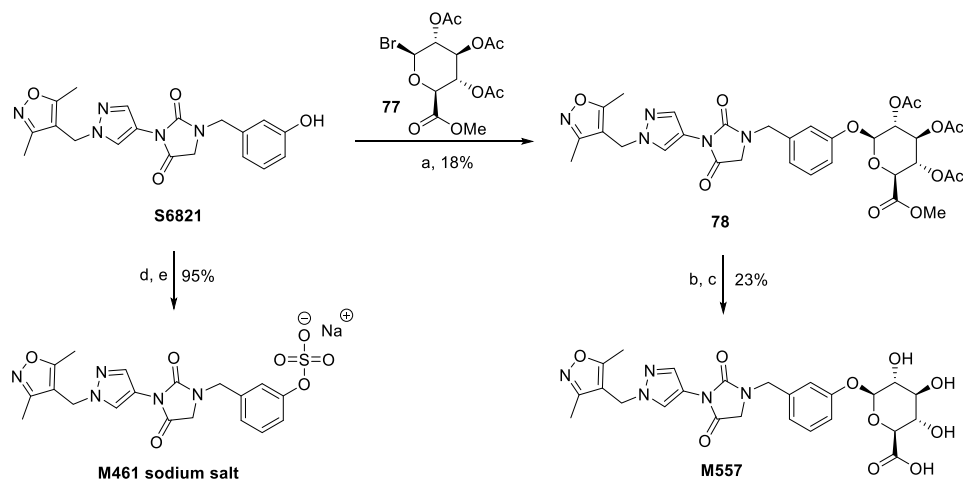
levels of intake by the Joint FAO/WHO Expert Committee on Food Additives and were assigned JECFA Nos. 2161 and 2162,<sup>85</sup> respectively. In addition, the Panel on Food Contact Materials, Enzymes, Flavorings and Processing Aids of The European Food Safety Authority (EFSA) has determined that S6821 (FL-no, 16.127) is not expected to be of a safety concern when used at levels up to those specified in different foods.<sup>86</sup> Regulatory jurisdictions in countries such as Japan, Korea, and Mexico (794 DO 5.9.2013) have also approved the use of S6821.

## CONCLUSION

We have disclosed a new class of 3-(pyrazol-4-yl)-imidazolidine-2,4-diones as potent, selective, and efficacious TAS2R8 antagonists. These include 3-(1-((3,5-dimethylisoxazol-4-yl)-methyl)-1H-pyrazol-4-yl)-1-(3-hydroxybenzyl)imidazolidine-2,4-dione (S6821) and 3-(1-((3,5-dimethylisoxazol-4-yl)-methyl)-1H-pyrazol-4-yl)-1-(3-hydroxybenzyl)-5,5-dimethylimidazolidine-2,4-dione (S7958), which have demonstrated the ability to significantly reduce the bitterness elicited by coffee. We demonstrated that the bitter fractions from roasted coffee extracts strongly activate TAS2R8. Thus, it is expected that S6821 and S7958 will also be effective in blocking TAS2R8-mediated bitterness associated with other products such as APIs, excipients, foods, beverages, and nutraceuticals. S6821 and S7958 have been tested in a panel of toxicity studies and were determined by US, Europe, and other national and global regulatory expert panels to be safe under intended conditions of use as bitter antagonists. Driven by this successful story, we are currently pursuing the identification and optimization of antagonists for other TAS2Rs.

## EXPERIMENTAL SECTION

**Biology. Ratiometric Calcium Imaging Methods.** Recombinant cells stably expressing TAS2R8 were grown overnight on Matrgel-coated glass coverslips. Prior to imaging, cells were incubated with 3

Scheme 6. Synthesis of M461 Sodium Salt and M557<sup>a</sup>

<sup>a</sup>Reagents and conditions: (a) silver triflate, DCM, overnight; (b) NaOH, MeOH, overnight; (c) HCl, MeOH/H<sub>2</sub>O, (d) pyridine SO<sub>3</sub> (PySO<sub>3</sub>), DCM, reflux, 2 h; (e) NaHCO<sub>3</sub>.

## Agonist activity of S6821 on TAS2R stable cell lines

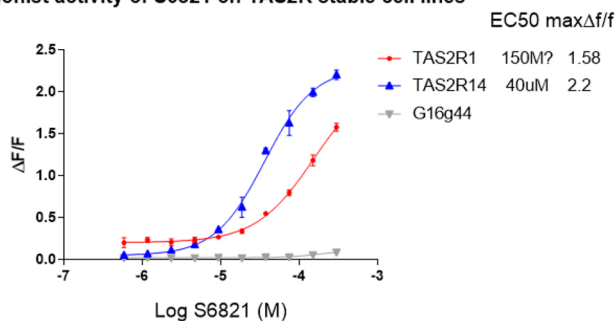


Figure 10. Dose–response evaluation of S6821 against TAS2R1 and TAS2R14.

Table 7. Perceived Bitterness Intensity Scores of S6821 on a Scale of 1–15<sup>a</sup>

treatment	average	standard deviation	Tukey's (5%) lettering
LSB + 50 μM S6821	1.0	1.0	A
LSB	1.6	2.1	Ab
LSB + 100 μM S6821	1.9	1.8	Ab
LSB + 150 μM S6821	2.8	3.1	B

<sup>a</sup>N = 30 responses (15 panelists × 2 replicates). Tukey's value = 1.155 (α = 0.05).

μg/mL FURA-2AM for 1 h at RT in HBSS. For imaging, cells were mounted on a fluorescent microscope equipped with a multichannel perfusion system and continuously perfused with HBSS and TAS2R8 agonist andrographolide (100 μM) or chloramphenicol (100 μM). For S6821 inhibition experiments, 1 μM of the inhibitor was applied for 60 s prior to and during agonist application. All compounds were prepared from DMSO stock, and the final DMSO concentrations did not exceed 0.1%. During acquisition, all cells in the field were autoselected by the software as regions of interest (ROIs) for analysis. Measurement of intracellular calcium levels were acquired at 1 Hz using 100 ms of excitation at 340 and 380 nm, and the emissions were monitored by a charge-coupled device (CCD) camera. The average response of all ROIs in the field and the peak responses for each cell were measured during each application. For S6821 recovery experiments, a 5 min wash-out period was determined sufficient for cells to fully recover from repetitive agonist stimulation, and only cells

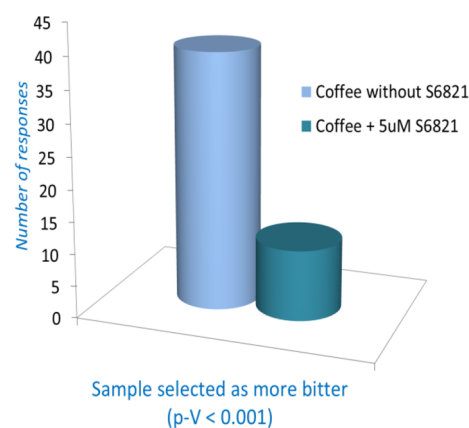


Figure 11. Number of responses selecting each sample as more bitter. N = 51 responses (17 panelists × 3 replicates).

## S7958 inhibition of andrographolide-induced response with TAS2R8

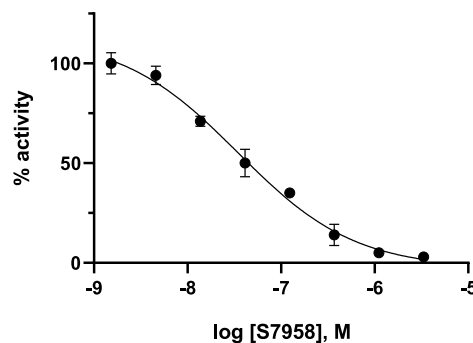
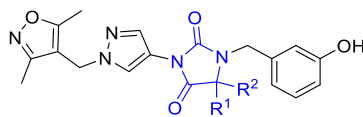


Figure 12. S7958 inhibition of TAS2R8 response to andrographolide.

with a strong initial TAS2R8 agonist responses (ΔF/F > 0.5) were selected for analysis.

**TAS2R8 Stable Cell Line.** Recombinant cells stably expressing the G protein chimera G16t44 and TAS2R8 were generated by transfection using standard lipofection techniques, and individual clones were isolated by limiting dilution. Clones were initially screened by responses to andrographolide in calcium imaging assays

Table 8. Selected Data for S6821 Analogues Targeting Stability Improvement



Cmpd	Hydantoin ring (varying R <sup>1</sup> and R <sup>2</sup> )	CLog	Solubility ( $\mu\text{M}$ ) <sup>a</sup>	TAS2R8 IC <sub>50</sub> ( $\mu\text{M}$ )	Sol./IC <sub>50</sub>	% Remaining <sup>b</sup>	
						pH 7.1	pH 2.8
S6821		-0.1	244	0.02	11619	55%	>99%
71		0.4	60	0.02	3750	92%	>99%
72		0.4	61	0.02	3389	92%	>99%
73		-0.6	2475	0.04	57558	2%	53%
S7958		0.9	72	0.06	1286	>99%	>99%
74		-0.1	356	0.1	2657	43%	>99%
75		0.2	31	0.02	1550	96%	>99%
76		0.7	3	0.04	77	98%	97%

<sup>a</sup>After 24 h at pH 7.1. <sup>b</sup>After 24 h at 100 °C.

Table 9. Number of Times Selected As More Bitter by Panelists<sup>a</sup>

samples	taste test with S6821	taste test with S7958
1.5× Alta Rica Course (ARC) + milk	40	33
1.5× ARC + milk + 5 $\mu\text{M}$ S6821	11	
1.5× ARC + milk + 5 $\mu\text{M}$ S7958		18
total responses	51	51
1.5× ARC + milk selected ( <i>p</i> - value)	<0.001	0.049

<sup>a</sup>*N* = 51 responses (17 panelists × 3 reps).

using fluo4-loaded cells on a fluorescent microscope. Clones showing the best response were characterized further on FLIPR.

**FLIPR Assay.** Recombinant cells stably expressing the TAS2R8 receptor were plated in a 384-well plate 24 h prior to the assay. On the day of the assay, the cells were incubated with fluo-4 dye in phosphate-buffered saline (PBS) for 60 min followed by 3 washes with PBS. Cells were subsequently resuspended in PBS and allowed to sit in the dark at room temperature for 15 min immediately prior to the assay. Compounds were diluted in PBS/DMSO at 2× the final assay concentration. The final DMSO concentration in the assay was 0.5%. For antagonist assays, the agonist and antagonist were premixed and added simultaneously. At the beginning of the assay, the baseline fluorescence was read on a fluorescence imaging plate reader (FLIPR, Molecular Devices) for 10 s prior to the addition of compounds. An equal volume of the compound was added to the cell plate, and changes in fluorescence were measured for an additional 100 s.

**Sensory Methods and Data Reporting.** The taste test and protocol used for evaluation by human panelists were reviewed and conducted according to guidance from external toxicology and regulatory experts in the field. Sensory evaluations were conducted after approval by the Firmenich Internal Review Board, and taste samples were only presented to panelists after written informed consent. The data and protocol packages associated with the title compounds have been reviewed by qualified regulatory authorities.

**Overview of Taste Test Methods.** Two different types of sensory tests were used to evaluate S6821 in either the inherent bitterness or blocking bitterness of coffee. The conducted taste tests include the following: (1) A sensory scaling test was performed using a 15-point bitterness scale in order to evaluate the reduction of bitterness intensity of S6821 alone. (2) A paired comparison test (2-alternative forced choice difference tests) was used to demonstrate a significant reduction in bitterness for coffee with S6821 added as compared to coffee alone.

**Stimuli.** Samples for the scaling evaluation were performed with solutions of S6821 at various concentrations (0, 100, and 150  $\mu\text{M}$ ). For these studies, S6821 was prepared as a concentrated stock solution in ethanol to ensure dissolution of the compound. Samples without compound within the same test were balanced with an equivalent concentration of ethanol. The final concentration of ethanol was 0.1%. Solutions were prepared in low sodium phosphate buffer (LSB; pH 7.1). LSB consists of 0.3 mM KCl, 0.5 mM Na<sub>2</sub>HPO<sub>4</sub>, and 0.175 mM KH<sub>2</sub>PO<sub>4</sub>.

Samples for the 2-alternative forced choice test (2-AFC) were performed with coffee samples prepared as follows: Alta Rica 100% Arabica instant coffee was prepared with 22.5 g of dry instant coffee in 750 mL of boiling water, to which 250 mL of whole milk was added

(control sample). The test sample used this same coffee preparation, to which the S6821 stock solution (see above) was added to make a final concentration of 5  $\mu$ M S6821.

**Subjects.** External trained panelists were used for both types of tests. Panelists have significant experience in evaluating bitterness intensity in various food products. Subjects were instructed not to eat or drink anything (except water) for at least 1 h prior to any test. Panelists were trained to use scaling procedures and were previously familiar with the sensory test methods used. The exact number of panelists used is reported with each test.

**Taste Test Procedures.** Panelists rinsed their mouths with water prior to starting any test. In scaling tests, panelists rated samples for bitterness. Samples were presented to panelists monadically, in a randomized, counterbalanced order. Panelists rinsed their mouths with water and had up to 1 min of delay to clear the mouth of any tastes after each evaluation. Two replicates of each test were performed. All samples were evaluated then expectorated (i.e., "sip and spit").

In the 2-AFC tests, panelists tasted pairs of solutions and indicated which sample was perceived to be more bitter. Pairs were provided in a randomized counterbalanced order and panelists completed three replicate tests. Between pairs, panelists rinsed with water and had up to a 1 min delay to clear the mouth of any tastes. Prior to the 2-AFC tests, the subjects were given a sample of the solution or product alone, and asked to describe its bitterness intensity using one of the following descriptors: none, barely detectable, weak, moderate, strong, and very strong.

**Sensory Data Reporting.** The statistical significance for scaling tests was calculated using a two-way ANOVA with interaction with  $\alpha = 0.05$ . The statistical significance for the 2-AFC tests was calculated using binomial probability tables for  $\alpha = 0.05$ .

**Chemistry. General Procedures.** The synthesis and characterization of **8**, **19**, and **23** (Table 1); **30**, **32** and **37** (Table 2); **S6821** and **S7958** (Table 8); **M397A**, **M397B**, and **M397C** (Scheme 5); and **M461 sodium salt** and **M557** (Scheme 6) are described below. The synthesis of all other compounds and their intermediates and corresponding characterization data are provided in the Supporting Information.

**Materials and Methods.** Unless otherwise noted, all compounds obtained from commercial sources were used without further purification. All tested compounds have a purity >95%, per one of the HPLC methods provided in the Supporting Information. The provided  $^1\text{H}$  NMR,  $^{13}\text{C}$  NMR, mass spectrometry (MS), and elemental analysis (EA) data were in all cases consistent with the proposed structures. For NMR, the chemical shifts ( $\delta$ ) are in ppm, and spectra were referenced using the residual solvent peak; coupling constants ( $J$ ) are in hertz. The following abbreviations were used for common solvents: deuterated dimethyl sulfoxide (DMSO- $d_6$ ) and deuterated chloroform ( $\text{CDCl}_3$ ). The description of  $^1\text{H}$  NMR peaks was performed using the following conventional abbreviations: singlet (s), doublet (d), triplet (t), quartet (q), multiplet (m), doublet of doublets (dd), doublet of triplets (dt), doublet of doublets of doublets (ddd), and broad (br). Mass spectra ( $m/z$ ) were recorded using electrospray ionization (ESI). Elemental Analyses were performed either by NuMega Resonance Laboratories or Exova Group plc.

**Ethyl 1-((3,5-Dimethylisoxazol-4-yl)methyl)-1H-pyrazole-4-carboxylate (3).** Ethyl 1H-pyrazole-4-carboxylate **1** (21 g, 147 mmol), 4-chloromethyl-3,5-dimethylisoxazole **2** (25 g, 172 mmol), and cesium carbonate (48 g, 147 mmol) were stirred in DMF (250 mL) under  $\text{N}_2$  at 80  $^\circ\text{C}$  for 16 h. The reaction mixture was cooled and filtered to remove inorganic salt. The liquid was diluted with 0.1 N HCl (200 mL) and then diluted with water (1 L) in which a white precipitate formed. The solid was collected by filtration, washed with water, and dried under a vacuum to afford the title compound **3** (35 g, 141 mmol, 97%) as a white solid.  $^1\text{H}$  NMR (DMSO- $d_6$ , 400 MHz):  $\delta$  1.25 (t,  $J = 7.2$  Hz, 3H), 2.14 (s, 3H), 2.41 (s, 3H), 4.20 (q,  $J = 7.2$  Hz, 2H), 5.20 (s, 2H), 7.86 (d,  $J = 0.8$  Hz, 1H), 8.43 (d,  $J = 0.8$  Hz, 1H). LC-MS (ESI):  $m/z$  250  $[\text{M} + \text{H}]^+$ .

**1-((3,5-Dimethylisoxazol-4-yl)methyl)-1H-pyrazole-4-carbohydrazide (4).** Ethyl 1-((3,5-dimethylisoxazol-4-yl)methyl)-1H-pyra-

zole-4-carboxylate **3** (86 g, 345 mmol) and hydrazine (110 g, 3454 mmol) were stirred in EtOH (1 L) at reflux for 48 h. LC-MS indicated that the reaction was complete at this point. The solution was concentrated under a vacuum, and the solid product was recrystallized from ethanol to afford the desired compound **4** (77 g, 328 mmol, 96%) as a white solid.  $^1\text{H}$  NMR (DMSO- $d_6$ , 400 MHz):  $\delta$  2.14 (s, 3H), 2.41 (s, 3H), 4.32 (br s, 2H), 5.17 (s, 2H), 7.83 (d,  $J = 0.8$  Hz, 1H), 8.18 (d,  $J = 0.8$  Hz, 1H), 9.31 (br s, 1H). LC-MS (ESI):  $m/z$  236  $[\text{M} + \text{H}]^+$ .

**1-((3,5-Dimethylisoxazol-4-yl)methyl)-1H-pyrazole-4-carbonyl Azide (5).** Note that the product **5** must be handled with care. Although we did not experience any issues with the acyl azide product **5**, such azide materials are known to decompose violently when friction and/or shock are applied.

Sodium nitrite (14 g, 202 mmol) in  $\text{H}_2\text{O}$  (700 mL) was added dropwise over 30 min to a solution of 1-((3,5-dimethylisoxazol-4-yl)methyl)-1H-pyrazole-4-carbohydrazide **4** (31.6 g, 134 mmol) in 10% aqueous acetic acid (2 L) at 0  $^\circ\text{C}$  (ice water bath). The reaction mixture became cloudy with a white precipitate during the addition of sodium nitrite. After the addition, the ice bath was removed, and the reaction mixture was stirred for an additional 30 min and was then allowed to warm to room temperature. The mixture was extracted with ethyl acetate (3 $\times$ , 300 mL). The combined organic extract was washed successively with aqueous saturated sodium carbonate, water, and brine. The organic phase was dried over sodium sulfate, filtered, and concentrated on a rotovap. The residue was recrystallized from ethanol to afford compound **5** (31 g, 126 mmol, 93%) as a white solid.  $^1\text{H}$  NMR (DMSO- $d_6$ , 400 MHz):  $\delta$  2.15 (s, 3H), 2.42 (s, 3H), 5.23 (s, 2H), 7.95 (d,  $J = 0.8$  Hz, 1H), 8.57 (d,  $J = 0.8$  Hz, 1H). LC-MS (ESI):  $m/z$  247  $[\text{M} + \text{H}]^+$ .

**1-((3,5-Dimethylisoxazol-4-yl)methyl)-1H-pyrazol-4-amine Hydrogen Chloride (6).** To a solution of **5** (1.00 g, 4.06 mmol) in anhydrous toluene were added 4  $\text{\AA}$  molecular sieves (MS) (2 g), and the mixture was refluxed for 2 h. After cooling to room temperature, *tert*-BuOH (50 mL) was added, and the mixture was heated again at reflux for 6 h. The reaction mixture was cooled to room temperature, filtered over a pad of celite, and the solvent was removed under a vacuum; the residue was triturated in hot  $\text{Et}_2\text{O}$ . The impurity that precipitated was filtered off, and the ethereal filtrate was dried on the rotovap to furnish *tert*-butyl 1-((3,5-dimethylisoxazol-4-yl)methyl)-1H-pyrazol-4-yl)carbamate (LC-MS (ESI):  $m/z$  293  $[\text{M} + \text{H}]^+$ ). The latter carbamate intermediate was dissolved without further purification in anhydrous methanol (50 mL) and treated with HCl in  $\text{Et}_2\text{O}$  (10 equiv). The mixture was refluxed for 2 h and concentrated under a vacuum to give a residue that was recrystallized from MeOH/ $\text{Et}_2\text{O}$  to afford the desired amine hydrochloric acid **6** as a whitish solid (0.70 g, 3.06 mmol, 75% over two steps).  $^1\text{H}$  NMR (DMSO- $d_6$ , 400 MHz):  $\delta$  2.14 (s, 3H), 2.41 (s, 3H), 5.18 (s, 2H), 7.54 (d,  $J = 0.8$  Hz, 1H), 8.03 (d,  $J = 0.8$  Hz, 1H), 10.12 (br s, 3H). LC-MS (ESI):  $m/z$  193  $[\text{M}_{\text{free base}} + \text{H}]^+$ . HPLC purity >95%.

**General Procedure A: N-1-((3,5-Dimethylisoxazol-4-yl)methyl)-1H-pyrazol-4-yl)picolinamide (8).** The amine hydrochloride **6** (400 mg, 2.1 mmol), picolinic acid (256 mg, 2.1 mmol), and HOBT (388 mg, 2.50 mmol) were mixed in dichloromethane (7 mL). The reaction mixture was treated with triethylamine (670 mL, 4.8 mmol) and then stirred for 15 min at room temperature under a nitrogen atmosphere. Then, EDC (598 mg, 3.1 mmol) was added, and the reaction mixture was continued to be stirred for an additional 4 h. The reaction mixture was then diluted with dichloromethane (5 mL), washed with a saturated  $\text{NaHCO}_3$  solution (2  $\times$  5 mL), and washed with a saturated NaCl solution (5 mL). The organic layer was collected, dried over sodium sulfate, filtered, and evaporated on the rotovap. The crude product was purified by reverse phase HPLC ( $\text{H}_2\text{O}$ /acetonitrile 10 to 90%) to afford the title compound **8** as a white solid (374.6 mg, 1.26 mmol, 60%).  $^1\text{H}$  NMR ( $\text{CDCl}_3$ , 400 MHz):  $\delta$  2.21 (s, 3H), 2.44 (s, 3H), 5.05 (s, 2H), 7.49–7.47 (m, 1H), 7.60 (d,  $J = 0.8$  Hz, 1H), 7.93–7.88 (dt,  $J = 14, 2$  Hz, 1H), 8.07 (s, 1H), 8.24–8.21 (d,  $J = 8.0$  Hz, 1H), 8.61–8.56 (m, 1H), 9.83 (bs, 1H). LC-MS (ESI):  $m/z$  298  $[\text{M} + \text{H}]^+$ . MP: 135–137  $^\circ\text{C}$ .

**General Procedure B:** *N*-(1-((3,5-Dimethylisoxazol-4-yl)methyl)-1H-pyrazol-4-yl)-3-hydroxybenzamide (**19**). The amine hydrochloride **6** (227 mg, 1.0 mmol), 3-hydroxybenzoic acid (138 mg, 1.0 mmol), PyBop (624 mg, 1.2 mmol), and triethylamine (0.28 mL, 2.0 mmol) were stirred in dimethylformamide (2 mL) at ambient temperature for 8 h under a nitrogen atmosphere. The mixture was diluted with ethyl acetate (3 mL) and washed, successively, with a saturated NaHCO<sub>3</sub> solution (2 × 3 mL) and a saturated NaCl solution (3 mL). The organic phase was collected, dried over anhydrous Na<sub>2</sub>SO<sub>4</sub>, filtered, and concentrated on a rotovap. The residue was dissolved in methanol (3 mL) and purified by reverse phase HPLC (H<sub>2</sub>O/acetonitrile, 10/90%). The pure fractions were concentrated on the rotovap, and the product was recrystallized from ethanol to afford the title compound **19** as an off-white solid (180 mg, 0.58 mmol, 58%). <sup>1</sup>H NMR (DMSO-*d*<sub>6</sub>, 400 MHz): δ 2.15 (s, 3H), 2.41 (s, 3H), 5.14 (s, 2H), 6.93–6.95 (m, 1H), 7.27–7.36 (m, 3H), 7.58 (d, *J* = 0.8 Hz, 1H), 8.09 (d, *J* = 0.8 Hz, 1H), 9.72 (br s, 1H), 10.34 (br s, 1H). LC-MS (ESI): *m/z* 313 [M + H]<sup>+</sup>.

**General Procedure C:** *N*-(1-((3,5-Dimethylisoxazol-4-yl)methyl)-1H-pyrazol-4-yl)benzo[d][1,3]dioxole-5-carboxamide (**23**). A solution of the amine hydrochloride **6** (7.3 g, 31.7 mmol) in DCM (200 mL) was treated at 0 °C with triethylamine (6.9 g, 68 mmol). The mixture was stirred until the free amine was completely dissolved. Benzo[d][1,3]dioxole-5-carbonyl chloride (5.8 g, 32 mmol) in DCM (50 mL) was then added dropwise. When the addition was complete, the ice bath was removed, and the reaction mixture was stirred for 1 h. The mixture was washed with aqueous 1 N HCl (200 mL), and the aqueous phase was back extracted with DCM (2 × 75 mL). The combined organic extract was dried over sodium sulfate, filtered, and concentrated on a rotovap. The crude product was purified by silica gel chromatography (60% ethyl acetate in hexanes), and the resulting light yellow solid was crystallized from ethanol/H<sub>2</sub>O to afford the title compound **23** (4.9 g, 45%) as a white solid. <sup>1</sup>H NMR (DMSO-*d*<sub>6</sub>, 400 MHz): δ 2.15 (s, 3H), 2.41 (s, 3H), 5.14 (s, 2H), 6.12 (s, 2H), 7.04 (d, *J* = 8.4 Hz, 1H), 7.47 (d, *J* = 1.6 Hz, 1H), 7.53 (dd, *J* = 8.4, 1.6 Hz, 1H), 7.57 (d, *J* = 0.8 Hz, 1H), 8.08 (d, *J* = 0.8 Hz, 1H), 10.26 (s, 1H). LC-MS (ESI): *m/z* 341 [M + H]<sup>+</sup>. MP: 172–173 °C.

**2-(1-((3,5-Dimethylisoxazol-4-yl)methyl)-1H-pyrazol-4-yl)isoindoline-1,3-dione (30)**. 2-(1H-pyrazol-4-yl)isoindoline-1,3-dione (1.5 g, 7 mmol), 4-(chloromethyl)-3,5-dimethylisoxazole (1.5 g, 10 mmol), and cesium carbonate (3.3 g, 10 mmol) were stirred in DMF (20 mL) at 80 °C for 3 h. The reaction mixture was cooled to room temperature, diluted with water (150 mL), and extracted with ethyl acetate (3 × 75 mL). The combined organic extract was dried over sodium sulfate, filtered, and concentrated on a rotovap. The solid product was triturated with ethyl acetate/Hexanes (1/9) and recrystallized from the refluxing ethanol (30 mL) to afford **30** (900 mg, 38%) as a bright, light yellow solid. <sup>1</sup>H NMR (DMSO-*d*<sub>6</sub>, 400 MHz): δ 2.18 (s, 3H), 2.43 (s, 3H), 5.24 (s, 2H), 7.83 (d, *J* = 0.8 Hz, 1H), 7.91–7.83 (m, 4H), 8.21 (d, *J* = 0.8 Hz, 1H). LC-MS (ESI): *m/z* 323 [M + H]<sup>+</sup>. MP: 170–171 °C.

***N*-(1-((3,5-Dimethylisoxazol-4-yl)methyl)-1H-pyrazol-4-yl)-2-phenylacetamide (32)**. A solution of amine hydrochloride **6** (230 mg, 1 mmol) and triethylamine (300 mg, 3 mmol) in DCM (10 mL) at 0 °C was treated dropwise with 2-phenylacetyl chloride (184 mg, 1.3 mmol). After the addition was complete, the reaction mixture was stirred for 1 h at room temperature. The mixture was diluted with DCM (50 mL) and washed with 1 N aqueous HCl (100 mL), followed by 1 N aqueous NaOH (100 mL) and water (100 mL). The combined organic extract was dried over sodium sulfate and filtered, and the solvent was removed under a vacuum. The resulting residue was purified by silica gel chromatography (50% ethyl acetate in hexanes) and triturated in ethyl acetate/hexanes (1/9) to afford compound **32** as a white solid (188 mg, 68%). <sup>1</sup>H NMR (CDCl<sub>3</sub>, 400 MHz): δ 2.15 (s, 3H), 2.38 (s, 3H), 3.69 (s, 2H), 4.96 (s, 2H), 7.15 (br s, 1H), 7.27–7.42 (m, 6H), 7.84 (s, 1H). LC-MS (ESI): *m/z* 311 [M + H]<sup>+</sup>. MP: 106–108 °C.

**General Procedure D:** 1-Benzyl-3-(1-((3,5-dimethylisoxazol-4-yl)methyl)-1H-pyrazol-4-yl)imidazolidine-2,4-dione (**37**). A solution of compound **48** (200 mg, 0.7 mmol), (bromomethyl)benzene **49**

(171 mg, 1 mmol), and cesium carbonate (325 mg, 1 mmol) in DMF (2 mL) was irradiated in the microwave reactor at 85 °C for 20 min. The reaction mixture was cooled to room temperature, diluted with aqueous 1 N HCl (100 mL), and extracted with ethyl acetate. The combined organic extract was dried over sodium sulfate, filtered, and concentrated. The residue was taken up in methanol (10 mL) and purified by reverse phase HPLC to afford the title compound **37** as an oily material that solidified upon standing (102 mg, 0.28 mmol, 40%).

<sup>1</sup>H NMR (CDCl<sub>3</sub>, 400 MHz): δ 2.19 (s, 3H), 2.42 (s, 3H), 3.85 (s, 2H), 4.62 (s, 2H), 5.06 (s, 2H), 7.40–7.27 (m, 5H), 7.92 (d, *J* = 0.8 Hz, 1H), 8.08 (d, *J* = 0.8 Hz, 1H). LC-MS (ESI): *m/z* 366 [M + H]<sup>+</sup>.

**3-(1-((3,5-Dimethylisoxazol-4-yl)methyl)-1H-pyrazol-4-yl)imidazolidine-2,4-dione (48)**. The acyl azide **5** (6 g, 25.5 mmol) in toluene (100 mL) was refluxed for 1 h and cooled to ambient temperature under a nitrogen atmosphere. Glycine methyl ester hydrochloride (3.1 g, 26 mmol) and triethylamine (3.2 g, 32 mmol) were added, and the mixture was refluxed for 16 h. The solvent was then removed under a vacuum, and the residue was dissolved in ethyl acetate (100 mL) and washed twice with a 1 N HCl solution (150 mL). The aqueous phase was back extracted with ethyl acetate (2 × 75 mL). The combined organic extract was dried over sodium sulfate, filtered, and concentrated on a rotovap. The resulting solid was triturated with ethyl acetate/hexanes (1/9) and dried under high vacuum to afford **48** as a white solid (5.2 g, 18.9 mmol, 74%). <sup>1</sup>H NMR (CDCl<sub>3</sub>, 400 MHz): δ 2.19 (s, 3H), 2.42 (s, 3H), 4.09 (d, *J* = 1.2 Hz, 2H), 5.06 (s, 2H), 5.68 (br s, 1H), 7.90 (d, *J* = 0.8 Hz, 1H), 8.05 (d, *J* = 0.8 Hz, 1H). LC-MS (ESI): *m/z* 276 [M + H]<sup>+</sup>.

**General Procedure E:** 3-(*tert*-Butyldimethylsilyloxy)benzaldehyde (**68a**). 3-Hydroxybenzaldehyde **67a** (30 g, 0.246 mmol) was dissolved in anhydrous DCM (350 mL), and imidazole (3 equiv) was added. The mixture was cooled to 0 °C, and a solution of *tert*-butylchlorodimethylsilane (1.3 equiv) in anhydrous DCM (250 mL) was added dropwise. After stirring overnight at room temperature, the reaction mixture was diluted with DCM (150 mL), washed with a 1 M aqueous HCl solution and brine, and dried over MgSO<sub>4</sub>. After filtration, the solvent was removed under reduced pressure, and the residue was purified over silica gel column using 3% EtOAc in hexanes to give the desired product **68a** in a quantitative yield (57.8 g). <sup>1</sup>H NMR (DMSO-*d*<sub>6</sub>, 400 MHz): δ 0.21 (s, 6H), 0.96 (s, 9H), 7.20 (ddd, *J* = 1.2, 2.4, 7.6 Hz, 1H), 7.31–7.34 (m, 1H), 7.47–7.56 (m, 2H), 9.96 (s, 1H). LC-MS (ESI): *m/z* 237 [M + H]<sup>+</sup>.

**2,3-Bis((*tert*-butyldimethylsilyloxy)benzaldehyde (68b)**. 2,3-Dihydroxybenzaldehyde **67b** (2.76 g, 20 mmol) and *tert*-butylchlorodimethylsilane (15.0 g, 5 equiv) were reacted according to general procedure E to afford the title compound **68b** (3.77 g, 52%). <sup>1</sup>H NMR (CDCl<sub>3</sub>, 400 MHz): δ 0.15 (s, 6H), 0.24 (s, 6H), 0.98 (s, 9H), 1.03 (s, 9H), 6.92 (br t, *J* = 8.0 Hz, 1H), 7.08 (dd, *J* = 2.0, 8.0 Hz, 1H), 7.41 (dd, *J* = 2.0, 8.0 Hz, 1H), 10.38 (s, 1H). LC-MS (ESI): *m/z* 367 [M + H]<sup>+</sup>.

**General Procedure F:** 2-(3-(*tert*-Butyldimethylsilyloxy)benzylamino)acetate (**70a**). To a solution of 3-(*tert*-butyldimethylsilyloxy)benzaldehyde **68a** (19.0 g, 80.38 mol) in anhydrous DCE (300 mL) were added methyl 2-aminoacetate hydrochloride **69a** (21 g, 16.73 mmol, 2 equiv), 4 Å MS (25 g), and Et<sub>3</sub>N (2.5 equiv). The mixture was stirred for 6 h at room temperature, cooled to 10 °C, and treated with NaBH(OAc)<sub>3</sub> (35 g, 16.51, ~ 2 equiv) while stirring vigorously. After the addition was completed, the cooling source was immediately removed, and the reaction mixture was stirred overnight under nitrogen. The mixture was quenched with a saturated aqueous NaHCO<sub>3</sub> solution, and the layers were separated. The aqueous phase was further extracted with DCM (2 × 300 mL). The combined organic extract was washed with water (50 mL) and brine (100 mL) and dried over MgSO<sub>4</sub>. The solvent was removed under a vacuum, and the residue was purified over silica gel using 25% ethyl acetate in hexanes to give the title compound **70a** (19.9 g, 64.30 mmol, 78%) as a colorless liquid. <sup>1</sup>H NMR (DMSO-*d*<sub>6</sub>, 400 MHz): δ 0.17 (s, 6H), 0.95 (s, 9H), 2.47 (br s, 1H), 3.28 (s, 2H), 3.62 (s, 3H), 3.65 (s, 2H), 6.70 (ddd, *J* = 0.8, 1.2, 8.0 Hz, 1H), 6.81 (m, 1H), 6.89 (dm, *J* = 7.6 Hz, 1H), 7.17 (*pseudo* t,

$J = 7.6, 8.0$  Hz, 1H). LC-MS (ESI):  $m/z$  247.1  $[M + H]^+$ . HPLC purity >95%. LC-MS (ESI):  $m/z$  310  $[M + H]^+$ .

**Ethyl 2-(3-(tert-butylidimethylsilyloxy)benzylamino)-2-methylpropanoate (70b).** Similar to general procedure F, to a solution of 3-(tert-butylidimethylsilyloxy)benzaldehyde **68a** (48.8 g, 0.206 mol) in anhydrous DCE (900 mL) were added ethyl 2-amino-2-methylpropanoate hydrochloride **69c** (86.3 g, 0.515 mol, 2.5 equiv), 4 Å MS (70 g), and Et<sub>3</sub>N (2.5 equiv). The mixture was stirred at room temperature overnight under nitrogen and then treated with NaBH(OAc)<sub>3</sub> (2 equiv); after the addition was completed, the reaction mixture was stirred overnight under nitrogen. The mixture was then diluted with DCM and carefully quenched with a saturated aqueous NaHCO<sub>3</sub> solution, and the layers were separated. The aqueous phase was further extracted with DCM. The combined organic extract was washed with water and brine, dried over MgSO<sub>4</sub>, and filtered. The solvent was removed under a vacuum, and the residue was purified over silica gel column using EtOAc/hexanes (2/8) to give the title compound **70b** (66.4 g, 92%). <sup>1</sup>H NMR (CDCl<sub>3</sub>, 400 MHz):  $\delta$  0.19 (s, 6H), 0.98 (s, 9H), 1.30 (t,  $J = 7.2$  Hz, 3H), 1.36 (s, 6H), 3.57 (s, 2H), 4.20 (q,  $J = 7.2$  Hz, 2H), 6.71 (ddd,  $J = 1.2, 2.4, 8.0$  Hz, 1H), 6.82 (m, 1H), 6.93 (dm,  $J = 7.6$  Hz, 1H), 7.16 (pseudo t,  $J = 7.6, 8.0$  Hz, 1H). LC-MS (ESI):  $m/z$  352  $[M + H]^+$ .

**Ethyl (2,3-Bis((tert-butylidimethylsilyloxy)benzyl)glycinate (70c).** 2,3-Bis((tert-butylidimethylsilyloxy)benzaldehyde **68b** (1.50 mg, 4.09 mmol) and ethyl 2-aminoacetate hydrochloride **69b** (3 equiv) were reacted according to general procedure F, and the product was purified over silica gel using 20% ethyl acetate in hexanes to afford the title compound **70c** (1.44 g, 3.17 mmol, 76%) as a yellowish oil. Anhydrous THF was used in lieu of DCE as the solvent. <sup>1</sup>H NMR (DMSO-*d*<sub>6</sub>, 400 MHz):  $\delta$  0.10 (s, 6H), 0.20 (s, 6H), 0.90 (s, 9H), 0.97 (s, 9H), 1.17 (t,  $J = 7.2$  Hz, 3H), 2.30 (br s, 1H), 3.25 (s, 2H), 3.67 (s, 2H), 4.06 (q,  $J = 7.2$  Hz, 2H), 6.76 (dd,  $J = 1.6, 8.0$  Hz, 1H), 6.82 (pseudo t,  $J = 7.6, 8.0$  Hz, 1H), 6.97 (dd,  $J = 1.6, 7.6$  Hz, 1H). LC-MS (ESI):  $m/z$  454  $[M + H]^+$ .

**General Procedure G: Ethyl (3,4-Bis((tert-butylidimethylsilyloxy)benzyl)glycinate (70d).** 3,4-Dihydroxybenzaldehyde **67c** (500 mg, 3.62 mmol) was dissolved in anhydrous DCM (100 mL), and imidazole (3.5 equiv) was added. The solution was cooled to 0 °C and treated with small portions of tert-butylchlorodimethylsilane (2.5 equiv). The reaction mixture was warmed slowly to room temperature, stirred overnight, and quenched with a 1 N HCl solution (2 equiv). The organic phase was washed with water and brine, dried over magnesium sulfate, and filtered. The filtrate was concentrated to afford a residue containing the protected aldehyde **68c** that was used in the next step without further purification. The residue was dissolved in anhydrous dichloroethane (100 mL), and ethyl 2-aminoacetate hydrochloride **69b** (2.5 equiv) was added, followed by treatment with TEA (2.5 equiv). Then, 4 Å MS (~1g) were added, and the mixture was stirred for 2 h at room temperature. The reaction mixture was cooled to about 10 °C, and while stirring vigorously, NaBH(OAc)<sub>3</sub> (2 equiv) was added. The reaction mixture was warmed slowly to room temperature and stirred overnight under nitrogen. The mixture was quenched with a saturated aqueous NaHCO<sub>3</sub> solution, and the layers were separated. The aqueous phase was further extracted with DCM (2 × 25 mL). The combined organic extract was washed with water (25 mL) and brine (50 mL) and dried over MgSO<sub>4</sub>. The solvent was removed under a vacuum, and the residue was purified over silica gel using 25% ethyl acetate in hexanes to afford the title compound **70d** (970 mg, 2.14 mmol, 59%, two steps) as a yellowish oil. <sup>1</sup>H NMR (CDCl<sub>3</sub>, 400 MHz):  $\delta$  0.18 (s, 6H), 0.19 (s, 6H), 0.98 (s, 18H), 1.27 (t,  $J = 7.2$  Hz, 3H), 3.37 (s, 2H), 3.67 (s, 2H), 4.19 (q,  $J = 7.2$  Hz, 2H), 7.72–7.81 (m, 3H). LC-MS (ESI):  $m/z$  454  $[M + H]^+$ .

**Ethyl (2,5-Bis((tert-butylidimethylsilyloxy)benzyl)glycinate (70e).** 2,5-Dihydroxybenzaldehyde **67e** (500 mg, 3.62 mmol), tert-butylchlorodimethylsilane (2.5 equiv), and ethyl 2-aminoacetate hydrochloride **69b** (3 equiv) were reacted according to general procedure G, and the product was purified over silica gel using 20% ethyl acetate in hexanes to afford the title compound **70e** (750 mg, 1.65 mmol, 46%, two steps) as a yellowish oil. <sup>1</sup>H NMR (CDCl<sub>3</sub>, 400

MHz):  $\delta$  0.16 (s, 6H), 0.20 (s, 6H), 0.97 (s, 9H), 1.00 (s, 9H), 1.26 (t,  $J = 7.2$  Hz, 3H), 3.36 (s, 2H), 3.73 (s, 2H), 4.16 (q,  $J = 7.2$  Hz, 2H), 6.59 (dd,  $J = 3.2, 8.4$  Hz, 1H), 6.65 (d,  $J = 8.4$  Hz, 1H), 6.74 (d,  $J = 3.2$  Hz, 1H). LC-MS (ESI):  $m/z$  454  $[M + H]^+$ .

**General Procedure H: 3-(1-((3,5-dimethylisoxazol-4-yl)methyl)-1H-pyrazol-4-yl)-1-(3-hydroxybenzyl)imidazolidine-2,4-dione (S6821).** This reaction was performed under N<sub>2</sub>. 1-((3,5-Dimethylisoxazol-4-yl)methyl)-1H-pyrazole-4-carbonyl azide **5** (38 g, 154 mmol) was stirred at reflux in dry toluene (600 mL) along with molecular sieves until no emission of nitrogen was observed, which indicates complete conversion of 1-((3,5-dimethylisoxazol-4-yl)methyl)-1H-pyrazole-4-carbonyl azide **5** into the 4-((4-isocyanato-1H-pyrazol-1-yl)methyl)-3,5-dimethylisoxazole intermediate. A solution of methyl 2-(3-(tert-butylidimethylsilyloxy)benzylamino)acetate **70a** (48 g, 154 mmol) in dry toluene (100 mL) was prepared. To this solution, the mixture obtained above, which contains the 4-((4-isocyanato-1H-pyrazol-1-yl)methyl)-3,5-dimethylisoxazole intermediate, was added, and the reaction mixture was refluxed for 48 h. The mixture was then allowed to cool to room temperature and was filtered over a pad of celite. The filtrate was concentrated on a rotovap, and the solid residue was suspended in methanol (1 L) and treated with HCl (2.0 M solution in diethyl ether, 540 mL). The solution was stirred for 16 h at 50 °C. The reaction mixture was partially concentrated on a rotovap to remove most of the diethyl ether, and the mixture diluted with water. The solid that formed was collected by filtration and recrystallized from hot ethanol (2 L). The product was collected by filtration and washed with ethanol to afford **S6821** (48 g, 127 mmol, 82%) as a white solid. <sup>1</sup>H NMR (DMSO-*d*<sub>6</sub>, 400 MHz):  $\delta$  2.15 (s, 3H), 2.41 (s, 3H), 3.99 (s, 2H), 4.45 (s, 2H), 5.21 (s, 2H), 6.64–6.77 (m, 3H), 7.11–7.19 (m, 1H), 7.80 (d,  $J = 0.8$  Hz, 1H), 8.19 (d,  $J = 0.4$  Hz, 1H), 9.44 (s, H). LC-MS (ESI):  $m/z$  382  $[M + H]^+$ . EA: calcd. C 59.84, H 5.02, N 18.36; found C 59.79, H 5.41, N 18.42.

**General Procedure I: 3-(1-((3,5-Dimethylisoxazol-4-yl)methyl)-1H-pyrazol-4-yl)-1-(3-hydroxybenzyl)-5,5-dimethylimidazolidine-2,4-dione (S7958).** This condition was designed to avoid the isolation of the acyl azide. Sodium nitrite (17.5 g, 254 mmol) in ice water (390 mL) was added to 1-((3,5-dimethylisoxazol-4-yl)methyl)-1H-pyrazole-4-carbohydrazide **4** (39.8 g, 169 mmol), in 10% acetic acid (1000 mL) and an ice/water bath at a rate that maintained a temperature below 5 °C. The mixture was stirred for 2.5 h at room temperature and then extracted twice with DCM (375 mL, 150 mL). The organic layer was washed with aqueous potassium carbonate (25%, 200 mL), water (200 mL), and brine and was dried with magnesium sulfate. The magnesium sulfate was filtered out to give a solution of 1-((3,5-dimethylisoxazol-4-yl)methyl)-1H-pyrazole-4-carbonyl azide **5** in DCM. The solution was added continuously to a solution of ethyl 2-(3-(tert-butylidimethylsilyloxy)benzylamino)-2-methylpropanoate **70b** (59.4 g, 169 mmol) in anhydrous toluene (1300 mL) in the presence of 4 Å MS (21 g) preheated to 105 °C at a rate that maintained an internal reaction temperature between 95 and 105 °C. The DCM was allowed to distill off during the addition step. The mixture was then refluxed for 16 h. The MS were filtered out, and the solvent was removed under a vacuum to give a residue, which was dissolved in anhydrous methanol (700 mL). HCl was added (2 M in diethyl ether, 144 mL), and the mixture was heated at 65 °C for 3 h. The solvent was removed under a vacuum, and the product was recrystallized from ethanol (330 mL) to give **S7958** (63.8 g, 92%) as a white solid. <sup>1</sup>H NMR (DMSO-*d*<sub>6</sub>, 400 MHz):  $\delta$  1.31 (s, 6H), 2.16 (s, 3H), 2.42 (s, 3H), 4.47 (s, 2H), 5.20 (s, 2H), 6.65 (ddd,  $J = 0.8, 2.4, 8$  Hz, 1H), 6.75–6.83 (m, 2H), 7.11 (t,  $J = 8$  Hz, 1H), 7.83 (d,  $J = 0.4$  Hz, 1H), 8.21 (d,  $J = 0.8$  Hz, 1H), 9.36 (s, H). LC-MS:  $m/z$  410  $[M + H]^+$ . EA: calcd. C 61.60, H 5.66, N 17.10; found C 61.69, H 6.05, N 17.32.

**General Procedure J: 1-(2,5-Dihydroxybenzyl)-3-(1-((3,5-dimethylisoxazol-4-yl)methyl)-1H-pyrazol-4-yl)imidazolidine-2,4-dione (M397A).** 1-((3,5-Dimethylisoxazol-4-yl)methyl)-1H-pyrazole-4-carbonyl azide **5** (423 mg, 1.72 mmol) in dry toluene (100 mL) was treated with 4 Å MS, and the mixture stirred at reflux under nitrogen for 2 h. After cooling the reaction to room temperature, a solution of

ethyl (2,5-bis((*tert*-butyldimethylsilyloxy)benzyl)glycinate **70e** (910 mg, 2.01 mmol) in dry toluene (20 mL) was added. The mixture was stirred at room temperature for 2 h, heated to 100 °C, and stirred overnight. The reaction mixture was cooled to room temperature and filtered over a pad of celite. The filtrate was concentrated on a rotovap, and the residue purified over silica gel using 25% EtOAc in hexanes to furnish the 1-(2,5-bis((*tert*-butyldimethylsilyloxy)benzyl)-3-(1-((3,5-dimethylisoxazol-4-yl)methyl)-1*H*-pyrazol-4-yl)-imidazolidine-2,4-dione intermediate as a colorless oil (950 mg, 88%) (LC-MS (ESI): *m/z* 626 [M + H]<sup>+</sup>). The latter intermediate (850 mg, 1.36 mmol) was then dissolved in methanol (25 mL) and treated with HCl (2 M in Et<sub>2</sub>O, 10 equiv). The reaction mixture was refluxed for 2 h, and the volatiles were removed under a vacuum. The residual solid was recrystallized from ethanol to afford the title compound **M397A** (295 mg, 0.74 mmol, 54%) as a whitish solid. <sup>1</sup>H NMR (DMSO-*d*<sub>6</sub>, 400 MHz): δ 2.14 (s, 3H), 2.41 (s, 3H), 4.01 (s, 2H), 4.40 (s, 2H), 5.20 (s, 2H), 6.51 (dd, *J* = 2.8, 8.4 Hz, 1H), 6.57 (d, *J* = 3.2 Hz, 1H), 6.65 (d, *J* = 8.4 Hz, 1H), 7.79 (d, *J* = 0.8 Hz, 1H), 8.19 (d, *J* = 0.8 Hz, 1H), 8.70 (s, 1H), 8.94 (s, H). LC-MS (ESI): *m/z* 382 [M + H]<sup>+</sup>. LC-MS (ESI): *m/z* 398 [M + H]<sup>+</sup>.

1-(3,4-Dihydroxybenzyl)-3-(1-((3,5-dimethylisoxazol-4-yl)methyl)-1*H*-pyrazol-4-yl)imidazolidine-2,4-dione (**M397B**). The title compound **M397B** (whitish solid, 300 mg, 0.66 mmol, 46%) was synthesized according to general procedure J from **70d** and the azide **5**. <sup>1</sup>H NMR (DMSO-*d*<sub>6</sub>, 400 MHz): δ 2.15 (s, 3H), 2.41 (s, 3H), 3.94 (s, 2H), 4.35 (s, 2H), 5.20 (s, 2H), 6.57 (dd, *J* = 2.0, 8.0 Hz, 1H), 6.67–6.73 (m, 2H), 7.79 (s, 1H), 8.18 (s, H), 8.93 (s, 1H), 8.94 (s, H). LC-MS (ESI): *m/z* 382 [M + H]<sup>+</sup>. LC-MS (ESI): *m/z* 398 [M + H]<sup>+</sup>.

1-(2,3-Dihydroxybenzyl)-3-(1-((3,5-dimethylisoxazol-4-yl)methyl)-1*H*-pyrazol-4-yl)imidazolidine-2,4-dione (**M397C**). The title compound **M397C** (whitish solid, 675 mg, 1.70 mmol, 62%) was synthesized according to general procedure J from **70c** and the azide **5**. <sup>1</sup>H NMR (DMSO-*d*<sub>6</sub>, 400 MHz): δ 2.14 (s, 3H), 2.40 (s, 3H), 3.99 (s, 2H), 4.47 (s, 2H), 5.20 (s, 2H), 6.55–6.67 (m, 2H), 6.75 (dd, *J* = 2.0, 7.2 Hz, 1H), 7.79 (d, *J* = 0.4 Hz, 1H), 8.18 (d, *J* = 0.8 Hz, 1H), 8.55 (br s, 2H). LC-MS (ESI): *m/z* 382 [M + H]<sup>+</sup>. LC-MS (ESI): *m/z* 398 [M + H]<sup>+</sup>.

Sodium 3-((3-(1-((3,5-Dimethylisoxazol-4-yl)methyl)-1*H*-pyrazol-4-yl)-2,4-dioxoimidazolidin-1-yl)methyl)phenyl Sulfate (**M461 Sodium Salt**). A solution of 3-(1-((3,5-dimethylisoxazol-4-yl)methyl)-1*H*-pyrazol-4-yl)-1-(3-hydroxybenzyl)imidazolidine-2,4-dione **S6821** (1.00 g, 2.60 mmol) in anhydrous DCM (50 mL) was treated with PySO<sub>3</sub> (10 equiv), and the mixture was refluxed for 2 h, cooled to room temperature, and quenched with saturated NaHCO<sub>3</sub> (10 equiv). The mixture was then stirred for 1 h at room temperature, and MeOH (15 mL) was added. The solid was filtered, and the organic phase was concentrated. The residue was dissolved in 1/3 MeOH/DCM (30 mL); the solid was filtered, and the filtrate was concentrated again. The latter was repeated again, and the foamy residue was dissolved in EtOH and precipitated by the slow addition of Et<sub>2</sub>O. The solid was collected and dried under a vacuum to give the desired product **M461 sodium salt** as a white powder (1.20 g, 2.48 mmol, 95%). <sup>1</sup>H NMR (DMSO-*d*<sub>6</sub>, 400 MHz): δ 2.15 (s, 3H), 2.41 (s, 3H), 4.00 (s, 2H), 4.51 (s, 2H), 5.20 (s, 2H), 6.98–7.03 (dm, *J* = 7.6 Hz, 1H), 7.09–7.16 (m, 2H), 7.26 (br t, *J* = 8.0 Hz, 1H), 7.79 (d, *J* = 0.8 Hz, 1H), 8.20 (d, *J* = 0.8 Hz, 1H). LC-MS (ESI): *m/z* 398 [M + H]<sup>+</sup>.

(2*S*,3*S*,4*S*,5*R*,6*S*)-6-(3-((3-(1-((3,5-Dimethylisoxazol-4-yl)methyl)-1*H*-pyrazol-4-yl)-2,4-dioxoimidazolidin-1-yl)methyl)phenoxy)-3,4,5-trihydroxytetrahydro-2*H*-pyran-2-carboxylic Acid (**M557**). 3-(1-((3,5-Dimethylisoxazol-4-yl)methyl)-1*H*-pyrazol-4-yl)-1-(3-hydroxybenzyl)imidazolidine-2,4-dione **S6821** (1.00 g, 2.6 mmol) and (3*R*,4*S*,5*S*,6*S*)-2-bromo-6-(methoxycarbonyl)tetrahydro-2*H*-pyran-3,4,5-triyl triacetate **77** (1.34 g, 3.38 mmol, 1.3 equiv) were dissolved in anhydrous DCM (25 mL), and silver triflate (0.97 g, 3.38 mmol, 1.3 equiv) was added. The mixture was stirred overnight in darkness, and ETA (1 mL) was added. The solution was further stirred for 30 min and filtered through a pad of celite. The filtrate was concentrated, and the residue was purified on silica gel using hexanes and an EtOAc

gradient to give (2*S*,3*R*,4*S*,5*S*,6*S*)-2-(3-((3-(1-((3,5-dimethylisoxazol-4-yl)methyl)-1*H*-pyrazol-4-yl)-2,4-dioxoimidazolidin-1-yl)methyl)phenoxy)-6-(methoxycarbonyl)tetrahydro-2*H*-pyran-3,4,5-triyl triacetate intermediate **78** (306 mg, 439 μmol, 18%) as a white solid (LC-MS (ESI): *m/z* 698 [M + H]<sup>+</sup>). A solution of the latter (2*S*,3*R*,4*S*,5*S*,6*S*)-2-(3-((3-(1-((3,5-dimethylisoxazol-4-yl)methyl)-1*H*-pyrazol-4-yl)-2,4-dioxoimidazolidin-1-yl)methyl)phenoxy)-6-(methoxycarbonyl)tetrahydro-2*H*-pyran-3,4,5-triyl triacetate intermediate (300 mg, 430 μmol) in methanol (5 mL) was treated with 2 N NaOH (10 equiv) and stirred overnight at room temperature. The reaction mixture was then acidified to pH 3–4 using a 5 N HCl solution, stirred for 30 min, and purified using reverse phase HPLC to furnish the desired product **M557** as a white solid (54 mg, 97 μmol, 23%). <sup>1</sup>H NMR (DMSO-*d*<sub>6</sub>, 400 MHz): δ 2.15 (s, 3H), 2.41 (s, 3H), 3.10–3.54 (m, 3H), 3.89 (d, *J* = 9.6 Hz, 1H), 4.01 (s, 2H), 4.52 (s, 2H), 5.07 (d, *J* = 7.6 Hz, 1H), 5.20 (s, 2H), 5.34 (m, 2H), 6.86–7.09 (m, 3H), 7.20–7.40 (m, 1H), 7.80 (d, *J* = 0.4 Hz, 1H), 8.19 (d, *J* = 0.8 Hz, 1H), 12.76 (s, 1H). LC-MS (ESI): *m/z* 558 [M + H]<sup>+</sup>.

## ■ ASSOCIATED CONTENT

### Supporting Information

The Supporting Information is available free of charge at <https://pubs.acs.org/doi/10.1021/acs.jmedchem.0c00388>.

Additional SAR table, experimental details, characterization data, and NMR spectral figures (PDF)

Molecular formula strings (CSV)

## ■ AUTHOR INFORMATION

### Corresponding Author

Joseph R. Fotsing – Firmenich SA, R&D North America, San Diego, California 92121, United States; [orcid.org/0000-0003-4223-7295](https://orcid.org/0000-0003-4223-7295); Email: [joseph.fotsing@firmenich.com](mailto:joseph.fotsing@firmenich.com), [jrfotsing@gmail.com](mailto:jrfotsing@gmail.com)

### Authors

Vincent Darmohusodo – Firmenich SA, R&D North America, San Diego, California 92121, United States

Andrew P. Patron – Firmenich SA, R&D North America, San Diego, California 92121, United States

Brett W. Ching – Firmenich SA, R&D North America, San Diego, California 92121, United States

Thomas Brady – Firmenich SA, R&D North America, San Diego, California 92121, United States

Melissa Arellano – Firmenich SA, R&D North America, San Diego, California 92121, United States

Qing Chen – Firmenich SA, R&D North America, San Diego, California 92121, United States

Timothy J. Davis – Firmenich SA, R&D North America, San Diego, California 92121, United States

Hanghui Liu – Firmenich SA, R&D North America, San Diego, California 92121, United States

Guy Servant – Firmenich SA, R&D North America, San Diego, California 92121, United States

Lan Zhang – Firmenich SA, R&D North America, San Diego, California 92121, United States

Mark Williams – Firmenich SA, R&D North America, San Diego, California 92121, United States

Michael Saganich – Firmenich SA, R&D North America, San Diego, California 92121, United States

Tanya Ditschun – Firmenich SA, R&D North America, San Diego, California 92121, United States

Catherine Tachdjian – Firmenich SA, R&D North America, San Diego, California 92121, United States

Donald S. Karanewsky – Firmenich SA, R&D North America, San Diego, California 92121, United States

Complete contact information is available at:  
<https://pubs.acs.org/10.1021/acs.jmedchem.0c00388>

## Notes

The authors declare the following competing financial interest(s): The authors work or have worked for Firmenich or its predecessor subsidiaries.

## ACKNOWLEDGMENTS

The authors thank Mr. Kenneth Simone for his diligence in getting the lead compounds evaluated by outside collaborators in formulations containing bitter APIs. The image used in the abstract graphic was downloaded free of charge from <https://dpng.com/png/1705614>. The authors thank DLPNG for allowing free download and use of the image.

## ABBREVIATIONS USED

TASxRy or TxRy, taste receptor y member x; OTOPI, otopetrin1; PKDxLy, polycystic kidney disease x-like y protein; ENaC, epithelial sodium channels; CCD, charge-coupled device; ROI, region of interest; HBSS, Hank's balanced salt solution; FLIPR, fluorescent imaging plate reader; dd, doublet of doublets; dt, doublet of triplets; ddd, doublet of doublets of doublets; br, broad; DIEA, *N,N*-diisopropylethylamine; EDCI, *N*-ethyl-*N'*-(3-(dimethylamino)propyl)carbodiimide hydrochloride; HOBt, hydroxybenzotriazole; NaBH(OAc)<sub>3</sub>, sodium triacetoxymethylborohydride; UHT, ultra-high-temperature processing; ANOVA, analysis of variance; 2-AFC, two-alternative forced choice; CD rat, Sprague–Dawley rat; WHO, World Health Organization; FAO, Food and Agriculture Organization; EFSA, European Food Safety Authority; FEMA, Flavor and Extract Manufacturers Association; GRAS, generally recognized as safe

## REFERENCES

- (1) Chandrashekar, J.; Hoon, M. A.; Ryba, N. J.; Zuker, C. S. The receptors and cells for mammalian taste. *Nature* **2006**, *444*, 288–294.
- (2) Chaudhari, N.; Roper, S. D. The cell biology of taste. *J. Cell Biol.* **2010**, *190*, 285–296.
- (3) Conte, C.; Ebeling, M.; Marcuz, A.; Nef, P.; Andres-Barquin, P. J. Identification and characterization of human taste receptor genes belonging to the TAS2R family. *Cytogenet. Genome Res.* **2002**, *98*, 45–53.
- (4) Kobayashi, Y.; Habara, M.; Ikezaki, H.; Chen, R.; Naito, Y.; Toko, K. Advanced taste sensors based on artificial lipids with global selectivity to basic taste qualities and high correlation to sensory scores. *Sensors* **2010**, *10*, 3411–3443.
- (5) Brockhoff, A.; Behrens, M.; Roudnitzky, N.; Appendino, G.; Avonto, C.; Meyerhof, W. Receptor agonism and antagonism of dietary bitter compounds. *J. Neurosci.* **2011**, *31*, 14775–14782.
- (6) Jaggupilli, A.; Singh, N.; De Jesus, V. C.; Gounni, M. S.; Dhanaraj, P.; Chelikani, P. Chemosensory bitter taste receptors (T2Rs) are activated by multiple antibiotics. *FASEB J.* **2019**, *33*, 501–517.
- (7) Meyerhof, W.; Batram, C.; Kuhn, C.; Brockhoff, A.; Chudoba, E.; Bufe, B.; Appendino, G.; Behrens, M. The molecular receptive ranges of human TAS2R bitter taste receptors. *Chem. Senses* **2010**, *35*, 157–170.
- (8) Teng, B.; Wilson, C. E.; Tu, Y. H.; Joshi, N. R.; Kinnamon, S. C.; Liman, E. R. Cellular and Neural Responses to Sour Stimuli Require the Proton Channel Otop1. *Curr. Biol.* **2019**, *29*, 3647–3656.
- (9) Zhang, J.; Jin, H.; Zhang, W.; Ding, C.; O'Keefe, S.; Ye, M.; Zuker, C. S. Sour Sensing from the Tongue to the Brain. *Cell* **2019**, *179*, 392–402.
- (10) Zhang, Y.; Hoon, M. A.; Chandrashekar, J.; Mueller, K. L.; Cook, B.; Wu, D.; Zuker, C. S.; Ryba, N. J. Coding of sweet, bitter, and umami tastes: different receptor cells sharing similar signaling pathways. *Cell* **2003**, *112*, 293–301.
- (11) Margolskee, R. F. Molecular mechanisms of bitter and sweet taste transduction. *J. Biol. Chem.* **2002**, *277*, 1–4.
- (12) Saotome, K.; Teng, B.; Tsui, C. C. A.; Lee, W. H.; Tu, Y. H.; Kaplan, J. P.; Sansom, M. S. P.; Liman, E. R.; Ward, A. B. Structures of the otopetrin proton channels Otop1 and Otop3. *Nat. Struct. Mol. Biol.* **2019**, *26*, 518–525.
- (13) Nelson, G.; Hoon, M. A.; Chandrashekar, J.; Zhang, Y.; Ryba, N. J.; Zuker, C. S. Mammalian sweet taste receptors. *Cell* **2001**, *106*, 381–390.
- (14) Chandrashekar, J.; Kuhn, C.; Oka, Y.; Yarmolinsky, D. A.; Hummler, E.; Ryba, N. J.; Zuker, C. S. The cells and peripheral representation of sodium taste in mice. *Nature* **2010**, *464*, 297–301.
- (15) Ishimaru, Y.; Inada, H.; Kubota, M.; Zhuang, H.; Tominaga, M.; Matsunami, H. Transient receptor potential family members PKD1L3 and PKD2L1 form a candidate sour taste receptor. *Proc. Natl. Acad. Sci. U. S. A.* **2006**, *103*, 12569–12574.
- (16) Horio, N.; Yoshida, R.; Yasumatsu, K.; Yanagawa, Y.; Ishimaru, Y.; Matsunami, H.; Ninomiya, Y. Sour taste responses in mice lacking PKD channels. *PLoS One* **2011**, *6*, No. e20007.
- (17) Tu, Y. H.; Cooper, A. J.; Teng, B.; Chang, R. B.; Artiga, D. J.; Turner, H. N.; Mulhall, E. M.; Ye, W.; Smith, A. D.; Liman, E. R. An evolutionarily conserved gene family encodes proton-selective ion channels. *Science* **2018**, *359*, 1047–1050.
- (18) Khan, S. I.; Della Santina, C. C.; Migliaccio, A. A. Angular vestibuloocular reflex responses in Otop1 mice. I. Otolith sensor input is essential for gravity context-specific adaptation. *J. Neurophysiol.* **2019**, *121*, 2291–2299.
- (19) Khan, S. I.; Della Santina, C. C.; Migliaccio, A. A. Angular vestibuloocular reflex responses in Otop1 mice. II. Otolith sensor input improves compensation after unilateral labyrinthectomy. *J. Neurophysiol.* **2019**, *121*, 2300–2307.
- (20) Adler, E.; Hoon, M. A.; Mueller, K. L.; Chandrashekar, J.; Ryba, N. J.; Zuker, C. S. A novel family of mammalian taste receptors. *Cell* **2000**, *100*, 693–702.
- (21) Behrens, M.; Foerster, S.; Staehler, F.; Raguse, J. D.; Meyerhof, W. Gustatory expression pattern of the human TAS2R bitter receptor gene family reveals a heterogeneous population of bitter responsive taste receptor cells. *J. Neurosci.* **2007**, *27*, 12630–12640.
- (22) Chandrashekar, J.; Mueller, K. L.; Hoon, M. A.; Adler, E.; Feng, L.; Guo, W.; Zuker, C. S.; Ryba, N. J. T2Rs function as bitter taste receptors. *Cell* **2000**, *100*, 703–711.
- (23) Matsunami, H.; Montmayeur, J. P.; Buck, L. B. A family of candidate taste receptors in human and mouse. *Nature* **2000**, *404*, 601–604.
- (24) Mueller, K. L.; Hoon, M. A.; Erlenbach, I.; Chandrashekar, J.; Zuker, C. S.; Ryba, N. J. The receptors and coding logic for bitter taste. *Nature* **2005**, *434*, 225–229.
- (25) Brockhoff, A.; Behrens, M.; Massarotti, A.; Appendino, G.; Meyerhof, W. Broad tuning of the human bitter taste receptor hTAS2R46 to various sesquiterpene lactones, clerodane and labdane diterpenoids, strychnine, and denatonium. *J. Agric. Food Chem.* **2007**, *55*, 6236–6243.
- (26) Fierro, F.; Giorgetti, A.; Carloni, P.; Meyerhof, W.; Alfonso-Prieto, M. Dual binding mode of “bitter sugars” to their human bitter taste receptor target. *Sci. Rep.* **2019**, *9*, 8437.
- (27) Sharma, P.; Yi, R.; Nayak, A. P.; Wang, N.; Tang, F.; Knight, M. J.; Pan, S.; Oliver, B.; Deshpande, D. A. Bitter Taste Receptor Agonists Mitigate Features of Allergic Asthma in Mice. *Sci. Rep.* **2017**, *7*, 46166.
- (28) Carey, R. M.; Workman, A. D.; Yan, C. H.; Chen, B.; Adappa, N. D.; Palmer, J. N.; Kennedy, D. W.; Lee, R. J.; Cohen, N. A.

- Sinonasal T2R-mediated nitric oxide production in response to *Bacillus cereus*. *Am. J. Rhinol Allergy* **2017**, *31*, 211–215.
- (29) Clark, A. A.; Dotson, C. D.; Elson, A. E.; Voigt, A.; Boehm, U.; Meyerhof, W.; Steinle, N. I.; Munger, S. D. TAS2R bitter taste receptors regulate thyroid function. *FASEB J.* **2015**, *29*, 164–172.
- (30) Dotson, C. D.; Vignes, S.; Steinle, N. I.; Munger, S. D. T1R and T2R receptors: the modulation of incretin hormones and potential targets for the treatment of type 2 diabetes mellitus. *Curr. Opin Investig Drugs* **2010**, *11*, 447–454.
- (31) Freund, J. R.; Lee, R. J. Taste receptors in the upper airway. *World J. Otorhinolaryngol Head Neck Surg* **2018**, *4*, 67–76.
- (32) Hinrichs, A. L.; Wang, J. C.; Bufe, B.; Kwon, J. M.; Budde, J.; Allen, R.; Bertelsen, S.; Evans, W.; Dick, D.; Rice, J.; Foroud, T.; Nurnberger, J.; Tischfield, J. A.; Kuperman, S.; Crowe, R.; Hesselbrock, V.; Schuckit, M.; Almasy, L.; Porjesz, B.; Edenberg, H. J.; Begleiter, H.; Meyerhof, W.; Bierut, L. J.; Goate, A. M. Functional variant in a bitter-taste receptor (hTAS2R16) influences risk of alcohol dependence. *Am. J. Hum. Genet.* **2006**, *78*, 103–111.
- (33) Maina, I. W.; Workman, A. D.; Cohen, N. A. The role of bitter and sweet taste receptors in upper airway innate immunity: Recent advances and future directions. *World J. Otorhinolaryngol Head Neck Surg* **2018**, *4*, 200–208.
- (34) Patel, N. N.; Workman, A. D.; Cohen, N. A. Role of Taste Receptors as Sentinels of Innate Immunity in the Upper Airway. *J. Pathog.* **2018**, *2018*, 9541987.
- (35) Lu, P.; Zhang, C. H.; Lifshitz, L. M.; ZhuGe, R. Extraoral bitter taste receptors in health and disease. *J. Gen. Physiol.* **2017**, *149*, 181–197.
- (36) Turner, A.; Veysey, M.; Keely, S.; Scarlett, C.; Lucock, M.; Beckett, E. L. Interactions between Bitter Taste, Diet and Dysbiosis: Consequences for Appetite and Obesity. *Nutrients* **2018**, *10*, 1336.
- (37) Liszt, K. I.; Ley, J. P.; Lieder, B.; Behrens, M.; Stoger, V.; Reiner, A.; Hochkogler, C. M.; Kock, E.; Marchiori, A.; Hans, J.; Widder, S.; Krammer, G.; Sanger, G. J.; Somoza, M. M.; Meyerhof, W.; Somoza, V. Caffeine induces gastric acid secretion via bitter taste signaling in gastric parietal cells. *Proc. Natl. Acad. Sci. U. S. A.* **2017**, *114*, E6260–E6269.
- (38) Liszt, K. I.; Hans, J.; Ley, J. P.; Kock, E.; Somoza, V. Characterization of Bitter Compounds via Modulation of Proton Secretion in Human Gastric Parietal Cells in Culture. *J. Agric. Food Chem.* **2018**, *66*, 2295–2300.
- (39) Lagerstrom, M. C.; Schiöth, H. B. Structural diversity of G protein-coupled receptors and significance for drug discovery. *Nat. Rev. Drug Discovery* **2008**, *7*, 339–357.
- (40) Kim, U.; Wooding, S.; Ricci, D.; Jorde, L. B.; Drayna, D. Worldwide haplotype diversity and coding sequence variation at human bitter taste receptor loci. *Hum. Mutat.* **2005**, *26*, 199–204.
- (41) Roudnitzky, N.; Risso, D.; Drayna, D.; Behrens, M.; Meyerhof, W.; Wooding, S. P. Copy Number Variation in TAS2R Bitter Taste Receptor Genes: Structure, Origin, and Population Genetics. *Chem. Senses* **2016**, *41*, 649–659.
- (42) Roudnitzky, N.; Behrens, M.; Engel, A.; Kohl, S.; Thalmann, S.; Hubner, S.; Lossow, K.; Wooding, S. P.; Meyerhof, W. Receptor Polymorphism and Genomic Structure Interact to Shape Bitter Taste Perception. *PLoS Genet.* **2015**, *11*, No. e1005530.
- (43) Roudnitzky, N.; Bufe, B.; Thalmann, S.; Kuhn, C.; Gunn, H. C.; Xing, C.; Crider, B. P.; Behrens, M.; Meyerhof, W.; Wooding, S. P. Genomic, genetic and functional dissection of bitter taste responses to artificial sweeteners. *Hum. Mol. Genet.* **2011**, *20*, 3437–3449.
- (44) Bufe, B.; Breslin, P. A.; Kuhn, C.; Reed, D. R.; Tharp, C. D.; Slack, J. P.; Kim, U. K.; Drayna, D.; Meyerhof, W. The molecular basis of individual differences in phenylthiocarbamide and propylthiouracil bitterness perception. *Curr. Biol.* **2005**, *15*, 322–327.
- (45) Kim, U. K.; Jorgenson, E.; Coon, H.; Leppert, M.; Risch, N.; Drayna, D. Positional cloning of the human quantitative trait locus underlying taste sensitivity to phenylthiocarbamide. *Science* **2003**, *299*, 1221–1225.
- (46) Pronin, A. N.; Xu, H.; Tang, H.; Zhang, L.; Li, Q.; Li, X. Specific alleles of bitter receptor genes influence human sensitivity to the bitterness of aloin and saccharin. *Curr. Biol.* **2007**, *17*, 1403–1408.
- (47) Soranzo, N.; Bufe, B.; Sabeti, P. C.; Wilson, J. F.; Weale, M. E.; Marguerie, R.; Meyerhof, W.; Goldstein, D. B. Positive selection on a high-sensitivity allele of the human bitter-taste receptor TAS2R16. *Curr. Biol.* **2005**, *15*, 1257–1265.
- (48) Roura, E.; Aldayyani, A.; Thavaraj, P.; Prakash, S.; Greenway, D.; Thomas, W. G.; Meyerhof, W.; Roudnitzky, N.; Foster, S. R. Variability in Human Bitter Taste Sensitivity to Chemically Diverse Compounds Can Be Accounted for by Differential TAS2R Activation. *Chem. Senses* **2015**, *40*, 427–435.
- (49) Bobowski, N.; Reed, D. R.; Mennella, J. A. Variation in the TAS2R31 bitter taste receptor gene relates to liking for the nonnutritive sweetener Acesulfame-K among children and adults. *Sci. Rep.* **2016**, *6*, 39135.
- (50) Poole, R. L.; Tordoff, M. G. The Taste of Caffeine. *J. Caffeine Res.* **2017**, *7*, 39–52.
- (51) Kim, U. K.; Breslin, P. A.; Reed, D.; Drayna, D. Genetics of human taste perception. *J. Dent. Res.* **2004**, *83*, 448–453.
- (52) Hayes, J. E.; Wallace, M. R.; Knopik, V. S.; Herbstman, D. M.; Bartoshuk, L. M.; Duffy, V. B. Allelic variation in TAS2R bitter receptor genes associates with variation in sensations from and ingestive behaviors toward common bitter beverages in adults. *Chem. Senses* **2011**, *36*, 311–319.
- (53) Drayna, D. Human taste genetics. *Annu. Rev. Genomics Hum. Genet.* **2005**, *6*, 217–235.
- (54) Pirastu, N.; Kooyman, M.; Robino, A.; van der Spek, A.; Navarini, L.; Amin, N.; Karssen, L. C.; Van Duijn, C. M.; Gasparini, P. Non-additive genome-wide association scan reveals a new gene associated with habitual coffee consumption. *Sci. Rep.* **2016**, *6*, 31590.
- (55) Pirastu, N.; Kooyman, M.; Traglia, M.; Robino, A.; Willems, S. M.; Pistis, G.; d'Adamo, P.; Amin, N.; d'Eustacchio, A.; Navarini, L.; Sala, C.; Karssen, L. C.; van Duijn, C.; Toniolo, D.; Gasparini, P. Association analysis of bitter receptor genes in five isolated populations identifies a significant correlation between TAS2R43 variants and coffee liking. *PLoS One* **2014**, *9*, No. e92065.
- (56) Wang, X.; Thomas, S. D.; Zhang, J. Relaxation of selective constraint and loss of function in the evolution of human bitter taste receptor genes. *Hum. Mol. Genet.* **2004**, *13*, 2671–2678.
- (57) Glendinning, J. I. Is the bitter rejection response always adaptive? *Physiol. Behav.* **1994**, *56*, 1217–1227.
- (58) Lindemann, B. Taste reception. *Physiol. Rev.* **1996**, *76*, 719–766.
- (59) Roy, G. M. The applications and future implications of bitterness reduction and inhibition in food products. *Crit. Rev. Food Sci. Nutr.* **1990**, *29*, 59–71.
- (60) Nissim, I.; Dagan-Wiener, A.; Niv, M. Y. The taste of toxicity: A quantitative analysis of bitter and toxic molecules. *IUBMB Life* **2017**, *69*, 938–946.
- (61) Drewnowski, A.; Gomez-Carneros, C. Bitter taste, phytonutrients, and the consumer: a review. *Am. J. Clin. Nutr.* **2000**, *72*, 1424–1435.
- (62) Lindemann, B. Receptors and transduction in taste. *Nature* **2001**, *413*, 219–225.
- (63) Thawabteh, A.; Lelario, F.; Scranò, L.; Bufo, S. A.; Nowak, S.; Behrens, M.; Di Pizio, A.; Niv, M. Y.; Karaman, R. Bitterless guaifenesin prodrugs-design, synthesis, characterization, in vitro kinetics, and bitterness studies. *Chem. Biol. Drug Des.* **2019**, *93*, 262.
- (64) Baguley, D.; Lim, E.; Bevan, A.; Pallet, A.; Faust, S. N. Prescribing for children - taste and palatability affect adherence to antibiotics: a review. *Arch. Dis. Child.* **2012**, *97*, 293–297.
- (65) Mennella, J. A.; Spector, A. C.; Reed, D. R.; Coldwell, S. E. The bad taste of medicines: overview of basic research on bitter taste. *Clin. Ther.* **2013**, *35*, 1225–1246.
- (66) Brockhoff, A.; Behrens, M.; Niv, M. Y.; Meyerhof, W. Structural requirements of bitter taste receptor activation. *Proc. Natl. Acad. Sci. U. S. A.* **2010**, *107*, 11110–11115.

- (67) Greene, T. A.; Alarcon, S.; Thomas, A.; Berdougo, E.; Doranz, B. J.; Breslin, P. A.; Rucker, J. B. Probenecid inhibits the human bitter taste receptor TAS2R16 and suppresses bitter perception of salicin. *PLoS One* **2011**, *6*, No. e20123.
- (68) Li, J.; Pan, L.; Fletcher, J. N.; Lv, W.; Deng, Y.; Vincent, M. A.; Slack, J. P.; McCluskey, T. S.; Jia, Z.; Cushman, M.; Kinghorn, A. D. In vitro evaluation of potential bitterness-masking terpenoids from the Canada goldenrod (*Solidago canadensis*). *J. Nat. Prod.* **2014**, *77*, 1739–1743.
- (69) Slack, J. P.; Brockhoff, A.; Batram, C.; Menzel, S.; Sonnabend, C.; Born, S.; Galindo, M. M.; Kohl, S.; Thalmann, S.; Ostopovici-Halip, L.; Simons, C. T.; Ungureanu, I.; Duineveld, K.; Bologna, C. G.; Behrens, M.; Furrer, S.; Oprea, T. I.; Meyerhof, W. Modulation of bitter taste perception by a small molecule hTAS2R antagonist. *Curr. Biol.* **2010**, *20*, 1104–1109.
- (70) Pydi, S. P.; Jaggupilli, A.; Nelson, K. M.; Abrams, S. R.; Bhullar, R. P.; Loewen, M. C.; Chelikani, P. Abscisic Acid Acts as a Blocker of the Bitter Taste G Protein-Coupled Receptor T2R4. *Biochemistry* **2015**, *54*, 2622–2631.
- (71) Pydi, S. P.; Sobotkiewicz, T.; Billakanti, R.; Bhullar, R. P.; Loewen, M. C.; Chelikani, P. Amino acid derivatives as bitter taste receptor (T2R) blockers. *J. Biol. Chem.* **2014**, *289*, 25054–25066.
- (72) Xu, Q.; Singh, N.; Hong, H.; Yan, X.; Yu, W.; Jiang, X.; Chelikani, P.; Wu, J. Hen protein-derived peptides as the blockers of human bitter taste receptors T2R4, T2R7 and T2R14. *Food Chem.* **2019**, *283*, 621–627.
- (73) Zhang, C.; Alashi, A. M.; Singh, N.; Liu, K.; Chelikani, P.; Aluko, R. E. Beef Protein-Derived Peptides as Bitter Taste Receptor T2R4 Blockers. *J. Agric. Food Chem.* **2018**, *66*, 4902–4912.
- (74) Jaggupilli, A.; Howard, R.; Upadhyaya, J. D.; Bhullar, R. P.; Chelikani, P. Bitter taste receptors: Novel insights into the biochemistry and pharmacology. *Int. J. Biochem. Cell Biol.* **2016**, *77*, 184–196.
- (75) Karanewsky, D. S.; Arthur, A. J.; Liu, H.; Chi, B.; Ida, L.; Markison, S. Toxicological evaluation of two novel bitter modifying flavour compounds: 3-(1-((3,5-dimethylisoxazol-4-yl)methyl)-1H-pyrazol-4-yl)-1-(3-hydroxybenzyl)imidazolidine-2,4-dione and 3-(1-((3,5-dimethylisoxazol-4-yl)methyl)-1H-pyrazol-4-yl)-1-(3-hydroxybenzyl)-5,5-dimethylimidazolidine-2,4-dione. *Toxicology reports* **2016**, *3*, 310–327.
- (76) Frank, O.; Zehentbauer, G.; Hofmann, T. Bioresponse-guided decomposition of roast coffee beverage and identification of key bitter compounds. *Eur. Food Res. Technol.* **2006**, *222*, 492–508.
- (77) Frank, O.; Blumberg, S.; Krumpel, G.; Hofmann, T. Structure determination of 3-O-caffeoyl-epi-gamma-quinide, an orphan bitter lactone in roasted coffee. *J. Agric. Food Chem.* **2008**, *56*, 9581–9585.
- (78) Frank, O.; Zehentbauer, G.; Hofmann, T. Screening and identification of bitter compounds in roasted coffee brew by taste dilution analysis. *Dev. Food Sci.* **2006**, *43*, 165–168.
- (79) Kostenis, E. Is G $\alpha$ 16 the optimal tool for fishing ligands of orphan G-protein-coupled receptors? *Trends Pharmacol. Sci.* **2001**, *22*, 560–564.
- (80) Ashby, J.; Tennant, R. W. Chemical structure, Salmonella mutagenicity and extent of carcinogenicity as indicators of genotoxic carcinogenesis among 222 chemicals tested in rodents by the U.S. NCI/NTP. *Mutat. Res., Genet. Toxicol. Test.* **1988**, *204*, 17–115.
- (81) Ashby, J.; Tennant, R. W.; Zeiger, E.; Stasiewicz, S. Classification according to chemical structure, mutagenicity to Salmonella and level of carcinogenicity of a further 42 chemicals tested for carcinogenicity by the U.S. National Toxicology Program. *Mutat. Res., Genet. Toxicol. Test.* **1989**, *223*, 73–103.
- (82) Tennant, R. W.; Ashby, J. Classification according to chemical structure, mutagenicity to Salmonella and level of carcinogenicity of a further 39 chemicals tested for carcinogenicity by the U.S. National Toxicology Program. *Mutat. Res., Rev. Genet. Toxicol.* **1991**, *257*, 209–227.
- (83) Marnett, L. J.; Cohen, S. M.; Fukushima, S.; Goodheram, N. J.; Hecht, S. S.; Riejtens, I. M. C. M.; Smith, R. L.; Adams, T. B.; Hallagan, J. B.; Harman, C.; McGowen, M. M.; Taylor, S. V. GRAS flavoring substances 26: The 26th publication by the Expert Panel of the Flavour and Extract Manufacturers Association provides an update on recent progress in the consideration of flavouring ingredients generally recognized as safe under the food additive amendment. *Food Technology* **2013**, *67*, 38–56.
- (84) Hallagan, J. B.; Hall, R. L. Under the conditions of intended use - New developments in the FEMA GRAS program and the safety assessment of flavor ingredients. *Food Chem. Toxicol.* **2009**, *47*, 267–278.
- (85) JEFCA. Safety Evaluation of certain Food Additives. Seventy-Sixth Meeting of the Joint FAO/WHO Expert Committee on Food Additives. *WHO Food Additives Series No.67*, 2012; 1–344.
- (86) Bolognesi, C.; Castle, L.; Cravedi, J.-P.; Engel, K. H.; Fowler, P.; Franz, R.; Grob, K.; Guertler, R.; Husoy, T.; Kaerenlampi, S.; Mennes, W.; Milana, R. M.; Penninks, A.; de Fatima Tavares Pocas, M.; Silano, V.; Smith, A.; Tlustos, C.; Woelfle, D.; Zorn, H.; Zugravu, C. A. Scientific opinion on Flavouring Group Evaluation 400 (FGE.400): 3-(1-((3,5-dimethylisoxazol-4-yl)methyl)-1H-pyrazol-4-yl)-1-(3-hydroxybenzyl)imidazolidine-2,4-dione. *EFSA Journal* **2016**, *14* (7), 4334.